UNIVERSIDADE FEDERAL DO PARANÁ

DIEGO TREVISAN MELFI

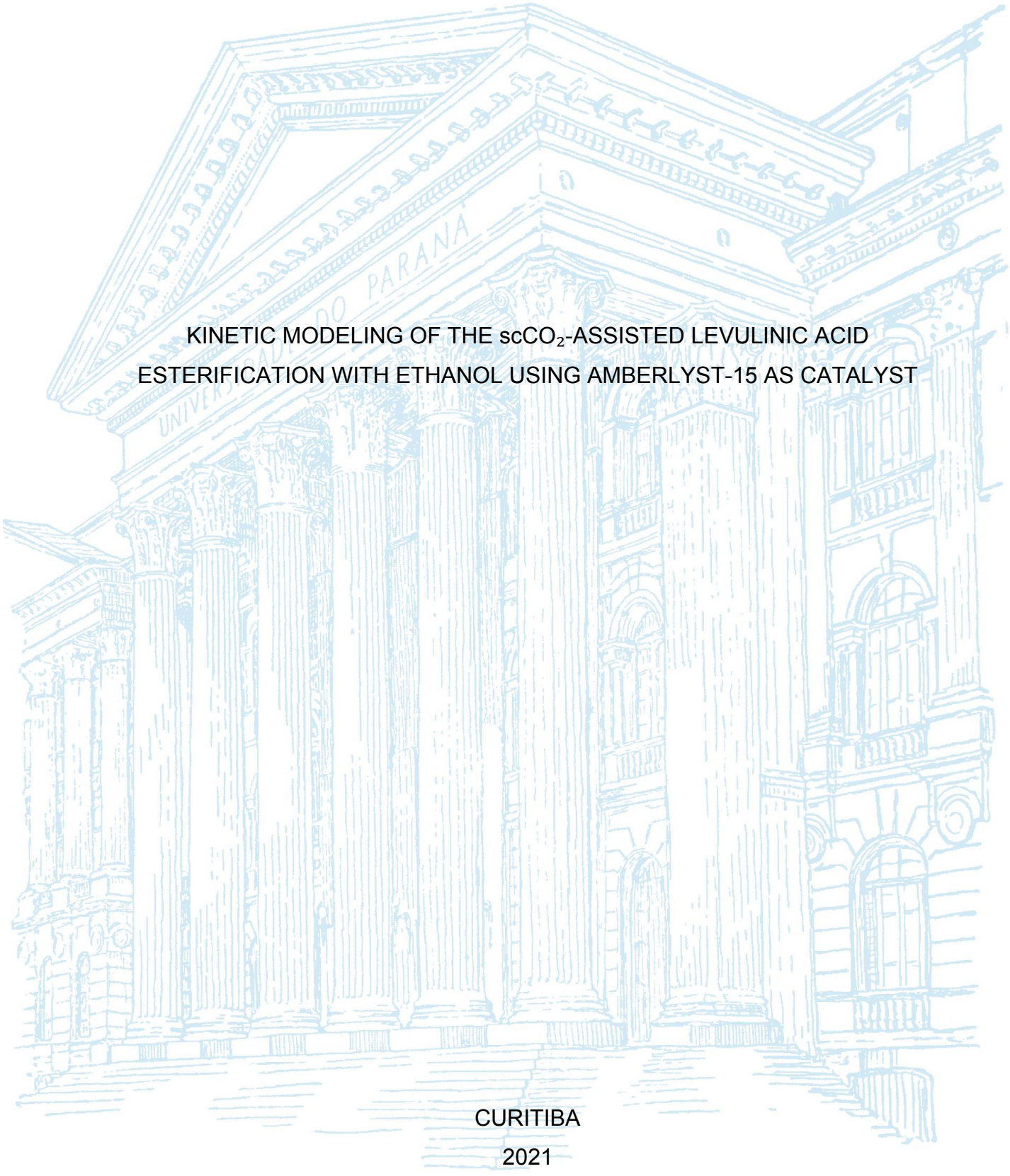

KINETIC MODELING OF THE $scCO_2$-ASSISTED LEVULINIC ACID ESTERIFICATION WITH ETHANOL USING AMBERLYST-15 AS CATALYST

CURITIBA

2021

DIEGO TREVISAN MELFI

KINETIC MODELING OF THE $scCO_2$-ASSISTED LEVULINIC ACID ESTERIFICATION WITH ETHANOL USING AMBERLYST-15 AS CATALYST

Dissertação apresentado como requisite parcial à obtenção do grau de Mestre em Engenharia Química no Curso de Pós-Graduação em Engenharia Química, Setor de Tecnologia, da Universidade Federal do Paraná

Orientador: Prof. Dr. Marcos Lúcio Corazza

Co-orientador: Prof. Dr. Marcelo Kaminski Lenzi

CURITIBA

2021

Catalogação na Fonte: Sistema de Bibliotecas, UFPR
Biblioteca de Ciência e Tecnologia

M245k Melfi, Diego Trevisan
Kinetic modeling of the $scCO_2$-assisted levulinic acid esterification with ethanol using amberlyst-15 as catalyst [recurso eletrônico] / Diego Trevisan Melfi – Curitiba, 2021.

Dissertação - Universidade Federal do Paraná, Setor de Tecnologia, Programa de Pós-graduação em Engenharia Química.
Orientador: Prof. Dr. Marcos Lúcio Corazza
Co-orientador: Prof. Dr. Marcelo Kaminski Lenzi

1. Esterificação (Química) 2. Dióxido de carbono. 3. Ácido levulínico. I. Universidade Federal do Paraná. II. Corazza, Marcos Lúcio. III. Lenzi, Marcelo Kaminski. IV. Título.

CDD: 660.2995

Bibliotecária: Roseny Rivelini Morciani CRB-9/1585

ATA Nº152

ATA DE SESSÃO PÚBLICA DE DEFESA DE MESTRADO PARA A OBTENÇÃO DO GRAU DE MESTRE EM ENGENHARIA QUÍMICA

No dia dezoito de maio de dois mil e vinte e um às 14:00 horas, na sala Microsoft Teams, Plataforma online, em função da portaria 754/2020 da Reitoria - UFPR, foram instaladas as atividades pertinentes ao rito de defesa de dissertação do mestrando **DIEGO TREVISAN MELFI**, intitulada**: Kinetic modeling of the scCO2-assisted levulinic acid esterification with ethanol using Amberlyst-15 as catalyst**. A Banca Examinadora, designada pelo Colegiado do Programa de Pós-Graduação em ENGENHARIA QUÍMICA da Universidade Federal do Paraná, foi constituída pelos seguintes Membros: MARCOS LÚCIO CORAZZA (UNIVERSIDADE FEDERAL DO PARANÁ), PAPA MATAR NDIAYE (UNIVERSIDADE FEDERAL DO RIO DE JANEIRO), ELITON FONTANA (UNIVERSIDADE FEDERAL DO PARANÁ). A presidência iniciou os ritos definidos pelo Colegiado do Programa e, após exarados os pareceres dos membros do comitê examinador e da respectiva contra argumentação, ocorreu a leitura do parecer final da banca examinadora, que decidiu pela APROVAÇÃO. Este resultado deverá ser homologado pelo Colegiado do programa, mediante o atendimento de todas as indicações e correções solicitadas pela banca dentro dos prazos regimentais definidos pelo programa. A outorga de título de mestre está condicionada ao atendimento de todos os requisitos e prazos determinados no regimento do Programa de Pós-Graduação. Nada mais havendo a tratar a presidência deu por encerrada a sessão, da qual eu, MARCOS LÚCIO CORAZZA, lavrei a presente ata, que vai assinada por mim e pelos demais membros da Comissão Examinadora.

CURITIBA, 18 de Maio de 2021.

Assinatura Eletrônica
14/06/2021 12:13:54.0
MARCOS LÚCIO CORAZZA
Presidente da Banca Examinadora (UNIVERSIDADE FEDERAL DO PARANÁ)

Assinatura Eletrônica
15/06/2021 16:48:03.0
PAPA MATAR NDIAYE
Avaliador Externo (UNIVERSIDADE FEDERAL DO RIO DE JANEIRO)

Assinatura Eletrônica
14/06/2021 08:57:56.0
ELITON FONTANA
Avaliador Interno (UNIVERSIDADE FEDERAL DO PARANÁ)

TERMO DE APROVAÇÃO

Os membros da Banca Examinadora designada pelo Colegiado do Programa de Pós-Graduação em ENGENHARIA QUÍMICA da Universidade Federal do Paraná foram convocados para realizar a arguição da Dissertação de Mestrado de **DIEGO TREVISAN MELFI** intitulada: **Kinetic modeling of the scCO2-assisted levulinic acid esterification with ethanol using Amberlyst-15 as catalyst**, que após terem inquirido o aluno e realizada a avaliação do trabalho, são de parecer pela sua APROVAÇÃO no rito de defesa.

A outorga do título de mestre está sujeita à homologação pelo colegiado, ao atendimento de todas as indicações e correções solicitadas pela banca e ao pleno atendimento das demandas regimentais do Programa de Pós-Graduação.

CURITIBA, 18 de Maio de 2021.

Assinatura Eletrônica
14/06/2021 12:13:54.0
MARCOS LÚCIO CORAZZA
Presidente da Banca Examinadora (UNIVERSIDADE FEDERAL DO PARANÁ)

Assinatura Eletrônica
15/06/2021 16:48:03.0
PAPA MATAR NDIAYE
Avaliador Externo (UNIVERSIDADE FEDERAL DO RIO DE JANEIRO)

Assinatura Eletrônica
14/06/2021 08:57:56.0
ELITON FONTANA
Avaliador Interno (UNIVERSIDADE FEDERAL DO PARANÁ)

ACKNOWLEDGEMENTS

I am thankful to my parents, Luciana and Paulo, who have always provided me the best formal and informal education; who have always supported and respected my decisions, even when they disagreed; and, more importantly, who have always raised me with love and care. I am thankful to my siblings, Fernanda and Thiago, who have always been my heroes while I grew up, and have always guided me, supported me, and helped me with pretty much anything that I needed. I am also thankful to my nephews: Gabriel, who has always been so kind and insightful, Felipe who has always been so cheerful and funny, and, Theo, who is still so young and yet is already so dear and amusing. It is a pleasure to watch you grow. My family has an enormous role in the building of who I am and in everything that I have achieved and will accomplish in my life.

I am also much thankful to my life partner, Estephanie. Our love and companionship were my fuels to complete this dissertation and to aim for bigger flights. Having her by my side since our first day as undergrads has made this journey way easier, joyful and exciting.

I am grateful to my main advisor, Corazza, who, in the last few years, has given me much more opportunities than I deserved, and to my co-advisor, Lenzi, who is to blame for my decision to pursue an academic career in the first place. They have taught me a lot about chemical engineering, research, teaching, and life.

I am grateful to my colleagues from LACTA, particularly, Amábille, Bruno, Damian, Fabi, Gabriela, Giulia, Julia, Kallynca, Kanda, Matheus, and Wanderson who have made my daily life in the lab as fun and enjoyable as possible, and to the visiting researches Eleni, Iohanna, Manuel, Margarita, Patricia, Stavros and Stefan who have made me see that it's a small world, after all.

I am grateful to Pré Escola Naviozinho, Colégio Stella Maris and Colégio Dom Bosco for my early childhood, primary and secondary education. I couldn't have asked for better teachers and friends in any of these schools. At last, but not least, I am grateful to the Federal University of Paraná, to the Department of Chemical Engineering and its secretary, Xisto, and to the Graduate Program in Chemical Engineering and its secretary, Cintya, for the excellent higher education, for the countless opportunities, and for being my second home over the last eight years.

Se você deixar de fazer alguma coisa que você ama porque você não quer morrer de fome, você vai morrer de tédio e de fome porque você vai ser um profissional incompetente. Mas se você escolher morrer de fome, você vai ser o melhor naquilo que faz e nunca vai morrer de tédio e muito menos de fome. Busque uma paixão, o que te fizer chorar é o sentido da sua vida.

Marcus Guilherme Bianco (1971-2021).

RESUMO

O levulinato de etila tem mostrado grande potencial como aditivo de combustível ambientalmente sustentável para gasolina, diesel e biodiesel. Uma alternativa para sua síntese é a esterificação direta do ácido levulínico com etanol, catalisada heterogeneamente. A maior parte dos processos catalíticos já relatados para este sistema, no entanto, depende de elevados tempos de residência para resultar em conversões apreciáveis de ácido levulínico. Este trabalho apresenta resultados experimentais e de modelagem da cinética da esterificação do ácido levulínico com etanol, catalisada por Amberlyst-15 e assistida por CO_2 supercrítico ($scCO_2$) em um reator batelada de volume fixo. São exploradas diferentes razões molares, quantidades de catalisador, temperaturas e cargas de $scCO_2$. O esquema de reação aqui apresentado leva a conversões de ácido levulínico próximas do equilíbrio após menos de 60 minutos na maioria das condições avaliadas. Para representar o comportamento de fase dos componentes na mistura reacional foi utilizada a equação de estado de Peng-Robinson com uma regra de mistura quadrática. Foi verificado que, na maioria das condições experimentais, a reação ocorre em um sistema bifásico devido ao uso de $scCO_2$, portanto, um algoritmo de flash *v-T* foi acoplado ao modelo cinético. A abordagem de modelagem proposta, que contempla a partição de fases dentro do reator, representa, até onde sabemos, uma das primeiras tentativas de simular esta promissora configuração de esterificação e pode ajudar no desenvolvimento futuro no campo emergente da catálise assistida por $scCO_2$. Adicionalmente, os dados experimentais e parâmetros cinéticos aqui reportados podem contribuir para na busca de um esquema de reação eficiente para a produção em larga escala de levulinato de etila.

Palavras-chave: Esterificação, CO_2 supercrítico, flash *v-T*, ácido levulínico, Amberlyst-15.

ABSTRACT

Ethyl levulinate has shown great potential as an environmentally sustainable fuel additive for gasoline, diesel and biodiesel. An alternative for its synthesis is the direct esterification of levulinic acid with ethanol, catalyzed heterogeneously. Most of the catalytic processes already reported for this system, however, depend on long residence times to result in appreciable conversions of levulinic acid. This work presents experimental results and modeling of the kinetics of the esterification of levulinic acid with ethanol, catalyzed by Amberlyst-15 and assisted by supercritical CO_2 ($scCO_2$) in a fixed volume batch reactor. Different molar ratios, catalyst amounts, temperatures and $scCO_2$ loads are explored. The reaction scheme presented here leads to levulinic acid conversions close to the equilibrium after less than 60 min in most of the conditions evaluated. To represent the phase behavior of the components in the reaction mixture, the Peng-Robinson equation of state with a quadratic mixing rule was used. It was found that, in most experimental conditions, the reaction occurs in a biphasic system due to the use of $scCO_2$, therefore, a *v-T* flash algorithm was coupled to the kinetic model. The proposed modeling approach, which contemplates the phase partition inside the reactor, represents, to the best of our knowledge, one of the first attempts to simulate this promising esterification configuration and may help in the future development in the emerging field of $scCO_2$-assisted catalysis. Additionally, the experimental data and kinetic parameters reported here may contribute to the search for an efficient reaction scheme for the large-scale production of ethyl levulinate.

Keywords: Esterification, supercritical CO_2, v-T flash, levulinic acid, Amberlyst-15.

FIGURES

TABLES

CONTENTS

1 INTRODUCTION

Ethyl levulinate is a biomass-derived ester with a wide variety of applications. Particularly stands out its potential as a green fuel additive for either gasoline (GHOSH *et al.*, 2018), diesel (WANG *et al.*, 2012), or biodiesel (JOSHI *et al.*, 2011). When added to fuels, ethyl levulinate can enhance engine efficiencies and reduce NOx and CO emissions (LEAL SILVA *et al.*, 2018). To effectively substitute some of the traditional fossil-derived fuel additives with ethyl levulinate, however, further efforts are need in developing and optimizing efficient processes. Hence, there is a pressing need to develop reaction approaches and conversion technologies to improve the ethyl levulinate production (LEAL SILVA *et al.*, 2018).

One possible chemical route to produce ethyl levulinate is the direct esterification of levulinic acid with ethanol. Esterification reactions have been of great commercial importance since the early 20th century (EMMET REID, 1937; OTERA; NISHIKIDO, 2010). Most esterification reactions are usually carried out in the presence of a catalyst (both homogenous and heterogeneous) (OTERA; NISHIKIDO, 2010) due to their slow reaction rates at mild temperature conditions. The levulinic acid esterification with ethanol is not an exception, Russo et al. (2018) found that under uncatalyzed conditions, at 90 °C and with an ethanol to levulinic acid molar ratio of 5:1, this reaction reaches only around 7 % of acid conversion after seven hours.

Inorganic acids are commonly applied as homogenous catalysts to perform esterification reactions, even in industrial scales (CHAI *et al.*, 2014). However, these processes have important drawbacks because most homogeneous catalysts are difficult to handle, have high corrosion potential and bring the need for additional downstream processing (COLE-HAMILTON, 2003; SIRSAM; HANSORA; USMANI, 2016). Heterogeneous catalysts, on the other hand, are easily handled and separated from the reaction products (SIRSAM; HANSORA; USMANI, 2016). However, heterogeneous catalysis is more susceptible to mass transfer limitations and catalyst deactivation due to the presence of a by-product or contaminant (SIEVERS *et al.*, 2016; WACŁAWEK; PADIL; CERNIK, 2018). Hence, the use of supercritical carbon dioxide ($scCO_2$) as solvent has been presented as an alternative to improves the reaction yields, minimizing the mass transfer limitations and leading

to higher effective reaction rates (SOH *et al.*, 2015; SUBRAMANLAMR; MCHUGH, 1986).

Although the technical feasibility of $scCO_2$ as solvent for some heterogeneously catalyzed esterification systems has been demonstrated in laboratory scales (MESHKSAR; AFSHARIANI; RAHIMPOUR, 2020), its industrial application still depends on process economic analysis, which, by its turn, depends on reliable modeling strategies. In this sense, this work investigates experimentally and computationally the kinetics of the $scCO_2$ assisted levulinic acid esterification with ethanol using Amberlyst-15 as catalyst, which is a promising reaction path for the ethyl levulinate production.

1.1 OBJECTIVES

The main goals of this work are: presenting experimental kinetic data for the levulinic acid esterification catalyzed by Amberlys-15 and assisted by $scCO_2$, and proposing a kinetic modeling strategy to contemplate the phase partition in $scCO_2$ reactions.

1.1.1 Specific objectives

To fulfill the main objectives of this work, the following specific objectives were set:

a) To compile binary vapor liquid equilibrium (VLE) data for the components at the reaction system (levulinic acid, ethanol, ethyl levulinate, water and CO_2) in a temperature/pressure range as close as the reaction conditions as possible.
b) To correlate the VLE data for these systems fitting binary interaction parameters for the Peng Robinson equation of state with a quadratic van der Waals mixing rule and Boston Mathias alpha function.
c) To collect unprecedent kinetic data for the $scCO_2$ assisted levulinic acid esterification with ethanol catalyzed by Amberlyst-15 in a wide range of process conditions.
d) To apply a *v-T* flash algorithm to calculate the phase partition inside the reaction vessel at the reaction conditions.

e) To propose a kinetic model that accounts for the phase partition inside the reactor to correlate the novel kinetic data.

2 LITERATURE REVIEW

This section aims to provide an overview of some materials and of the reaction studied in this work. Initially, some aspects about the physicochemical properties of levulinic acid and ethyl levulinate, as well as their role as chemical platform and biobased fuel additive, respectively, are presented. Further, a systematic review of the recent publications (from 2017-2021) available through the ScienceDirect platform regarding the esterification kinetics of the reaction between levulinic acid and ethanol is presented. Later it is given an overview on catalysis by ion-exchange resins. Finally, at the end of this section, the use of $scCO_2$ as solvent is discussed.

2.1 LEVULINIC ACID AND ETHYL LEVULINATE

Levulinic acid, also known as 4-oxopentanoic acid, is a short chain organic acid that presents two functional groups: a carboxyl and a carbonyl (see Figure 1). It is a colorless crystalline compound when pure, or a transparent to pale yellow colored liquid as commercial product. Its molar mass is 116.1 g/mol, its melting point ranges between 33 and 37 °C and its boiling point is 245 °C. v. Grote and Tollens (1874) credit the first preparations of levulinic acid to Malaguti in 1836 and Mulder in 1840 who heated sucrose with diluted sulfuric acid and isolated crude levulinic acid as a viscous oil (MASCAL; DUTTA, 2014).

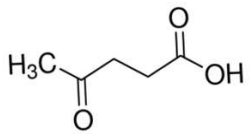

Figure 1: Molecular structure of levulinic acid.

Levulinic acid can be obtained from lignocellulosic materials such as corn starch, sugarcane bagasse, wheat straw, rice husks, paddy straw, sorghum grain, water hyacinth, paper mill sludge, tobacco chops, and olive tree pruning (GALLETTI *et al.*, 2012; MORONE; APTE; PANDEY, 2015). Due to its multifunctionality, levulinic acid has a wide scope of possibilities for chemical transformations and can be a precursor for several acids, ketones, esters, ethers and alcohols with vast applicability. Therefore, owing to its potential to serve as a green platform chemical,

levulinic acid has been selected by the US Department of Energy, with ethanol and other compounds, as part of the 15 carbohydrate-derived chemical building blocks for the development of biorefineries (BOZELL; PETERSEN, 2010).

Among the compounds that can be produced from levulinic acid, stands out the product of its esterification with ethanol, the ethyl levulinate. Ethyl levulinate can be used as a solvent, polymer plasticizer, flavorings, among others. However it has greater prominence as an oxygenated green fuel additive for either gasoline (GHOSH *et al.*, 2018), diesel (WANG *et al.*, 2012), or biodiesel (JOSHI *et al.*, 2011), because of its attractive physical properties for this end, such as: high lubricity, less toxicity, thermal stability and fluid dynamic stability in low temperatures (DÉMOLIS; ESSAYEM; RATABOUL, 2014).

Due to the great appealing of ethyl levulinate several studies have been performed so far to elucidate and optimize its chemical production pathways either from raw biomass (CHANG; XU; JIANG, 2012; LE VAN MAO *et al.*, 2011; OLSON, E.S., KJELDEN, R.K., SCHLAG; SHARMA, 2001), carbohydrates (GARVES, 1988; ZHAO *et al.*, 2015; ZHU *et al.*, 2014) or directly from levulinic acid, which is the subject of Section 2.2.

2.2 LEVULINIC ACID ESTERIFICATION WITH ETHANOL

The direct esterification of levulinic acid with ethanol (equation (1)) is a highly selective and attractive alternative for the synthesis of ethyl levulinate. Similar to most of the other esterification reactions, however, the ethanolic esterification of levulinic acid presents low reaction rates at mild temperature conditions. Russo et al. (2018) found that under uncatalyzed conditions, at 90 °C and with an ethanol to levulinic acid molar ratio of 5:1, this reaction reaches only around 7 % of acid conversion after seven hours. Therefore, this reaction is usually carried out in the presence of either homogeneous or heterogeneous catalysts.

$$\underset{(LA)}{Levulinic\ acid} + \underset{(EtOH)}{Ethanol} \rightleftarrows \underset{(EL)}{Ethyl\ Levulinate} + \underset{(W)}{Water} \tag{1}$$

Recent works (from 2017-2021) that concerned the catalyzed levulinic acid esterification were systematically reviewed to get an overview of the state-of-the-art

on the levulinic acid catalyzed esterification. The ScienceDirect platform was used to screen these studies considering the keywords levulinic acid, esterification, ethanol, ethyl levulinate, and catalyst. The initial search retrieved over 200 results, therefore only research articles whose main focus is the catalyzed levulinic acid esterification with ethanol were further considered, resulting in a total 22 papers in the last few years.

Most of these recent studies (13 of them) investigated novel catalysts to carry out this reaction and therefore are more focused on the catalyst characterization, stability and the effect of some process variables (BHAT; MAL; DUTTA, 2021; GADAMSETTI *et al.*, 2018; GUO; QIU; QI, 2019; IMYEN *et al.*, 2021; JIA; LIU; QI, 2020; KONG *et al.*, 2017; LUAN *et al.*, 2018; OGINO; SUZUKI; MUKAI, 2018; POPOVA *et al.*, 2018; SERT, 2020; ZAINOL *et al.*, 2017, 2019). Six of these studies (DA SILVA JUNIOR *et al.*, 2020a; RUSSO *et al.*, 2018, 2020a, 2020b; SALVI; YADAV, 2019; TSAI, 2014) reported, at different process conditions, experimental esterification kinetics of levulinic acid with ethanol, and only three of these six (RUSSO *et al.*, 2018, 2020a, 2020b) also presented a kinetic model to represent their data.

RUSSO *et al.* (2018) investigated the levulinic acid esterification kinetics using sulfuric acid and the ion-exchange resin Smopex-101 as catalysts. The authors proposed pseudo-homogeneous concentration-based kinetic models for both catalysts, however, it must be emphasized that while experiments at different temperatures have been carried out by the authors with sulfuric acid as catalyst, all experiments with Smopex-101 as catalyst were performed at 60 °C. Later, RUSSO *et al.* (2020a and 2020b) studied, respectively, the levulinic acid esterification kinetics using Amberlyst-15 and Amberlite IR120 as catalysts. The authors proposed detailed intraparticle diffusion models to represent their kinetic experiments and considered a pseudo-homogeneous concentration-based rate-law in both works. To validate their kinetic model, the authors carried reactions in continuous packed-bed reactors.

The three remaining studies (NOVITA; LEE; LEE, 2017; SHRIKHANDE *et al.*, 2020; VÁZQUEZ-CASTILLO *et al.*, 2019) are focused on process design and have proposed reactive distillation columns to perform the levulinic acid esterification. All of them have used the same catalyst (Amberlyst 39) and kinetic model to perform their calculations. However, it must be pointed out that while the experimental data originally used to fit this kinetic model was acquired in temperatures up to 75 °C

(TSAI, 2014), the three studies proposed operational temperatures higher than 80 °C for the top of the reactive distillation columns and higher than 100 °C for the bottom of the column. This sort of extrapolation might have resulted in unrealistic results in their simulations, although any of the authors have commented about it.

It is clear from this brief description of the recent works regarding the levulinic acid esterification that most studies have been focused on experimenting novel catalysts. Fewer have dedicated to perform kinetic studies and even fewer to investigate large scale process design alternatives. It seems that a time and cost-effective way to carry out this reaction is yet to be found, however, despite the intraparticle mass transfer limitations explored by (RUSSO *et al.*, 2020a, 2020b) in their works, ion exchange resins have been extensible studied for this system, being the object of the most advanced works towards a large-scale production of ethyl levulinate from levulinic acid so far.

2.3 ION-EXCHANGE RESINS

Ion exchange materials might be defined as insoluble matrices with labile cations or anions that are capable of exchanging ions with the medium where they are immerse without major structural changes. The idea that ion exchanger materials can be used to replace homogeneous catalysts dates back to the early 20th century. Typically, sulfonic acid cation exchangers and quaternary ammonium anion exchangers are used as resins to substitute mineral acids or bases as catalysts, respectively (CHAKRABARTI; SHARMA, 1993).

Concerning the resins' structure, although most materials are found as spherical beads of approximately the same size, the resins can be divided in two groups: gel and macroreticular resins. A gel bead is a homogeneous polymeric matrix on a microscopic scale. When the gel beads are dry, the polymeric matrix collapses and it does not exhibit significant catalytic activity unless at least one of the reactants is capable of swelling the matrix. This happens because only the sites on the bead's surface, which are a very small fraction of the total sites within the body bead, would be available to the reactants. Hence, the reactants swelling capacity play a major role when gel resins are used as catalysts (PITOCHELLI, 1980).

The advent of the macroreticular resins, around 1960, was a major breakthrough in the field of ion exchange catalysis because it overcame the

limitations regarding the swelling properties of the reactants, and largely expanded the application of ion exchange resins as catalysts. Unlike the gel resins, the macroreticular resins are heterogeneous on a microscopic scale. They are agglomerates of very small gel microspheres interspersed with macropores through which the reactants can easily move (PITOCHELLI, 1980).

The commercially available Amberlyst-15 is a particularly prominent macroreticular ion exchange resin for organic synthesis. It is a polystyrene-based cationic resin with strongly acidic sulfonic groups. Amberlyst-15 has been widely applied esterification reactions and have proven itself a powerful and selective catalyst for these transformations (PAL; SARKAR; KHASNOBIS, 2012). To our knowledge, so far, three studies have reported results for the levulinic acid esterification with ethanol.

RAMLI; ZAHARUDIN; AMIN (2017) investigated the effect of some process variables and the catalyst reusability for the levulinic acid esterification with methanol catalyzed by Amberlyst-15. As an additional comparison, the authors also performed reactions with ethanol and n-butanol as reactants. For the levulinic acid esterification with ethanol they obtained 71 % of levulinic acid conversion after 5h at reflux temperature (78.4 °C) with 20:1 ethanol to levulinic acid molar ratio and 30 wt% catalyst to levulinic acid mass proportion.

TROMBETTONI *et al.* (2017) studied in both batch and continuous systems the esterification of levulinic acid with n-pentanol using three different acidic resins: Amberlyst-15, polysterene-supported p-toluensulfonic acid, and Arquivion mP98. The authors also have reported in batch scheme results using different alcohols for the levulinic acid esterification catalyzed by Amberlyst-15. For ethanol, at 70 °C with 1:10 ethanol to levulinic acid molar ratio and 18.3 wt% catalyst to levulinic acid mass proportion they obtained 65 % of levulinic acid conversion after 24 hours.

As mentioned on the previous section, RUSSO *et al.* (2020a) have dedicated themselves to the study of levulinic acid esterification kinetics with ethanol and catalyzed by Amberlyst-15. The authors carried out batch esterification reactions over a wide range of process conditions: Temperatures from 50 to 90 °C, ethanol to levulinic acid molar ratios from 1:1 to 6:1 and catalyst to acid mass relations from around 4 wt% to around 16 wt%. They could describe their kinetic data using an intraparticle diffusion model and found that intraparticle diffusion limitations exist for this reaction. At 90 °C with an ethanol to levulinic acid molar ratio of 5:1 and around

8 wt% catalyst to acid mass relation, the authors found near equilibrium (around 88 %) levulinic acid conversions.

In light of the well-known intraparticle mass transfer limitations that the ion exchange resins might be subjected to (CHAKRABARTI; SHARMA, 1993), quantitatively explored by RUSSO *et al.* (2020a), it seems that the use of $scCO_2$ to overcome the mass transfer limitations might be a good direction to boost the use of Amberlyst-15 as catalyst for the esterification of levulinic acid with ethanol. As addressed in section 2.4, the use of $scCO_2$ as solvent is promising alternative to enhance mass transfer limited reactions and has attracted significant attention in the field of heterogeneous catalysis.

2.4 $scCO_2$ AS SOLVENT

Fluids near their critical point present intermediate properties between those in their liquid and those in their gaseous state. This unique combination of physical properties has been exploited in reaction engineering. Among the benefits of carrying reactions in supercritical media, one can highlight the high reaction rates, the improved selectivity and the reduction of mass transfer limitations (MAYADEVI, 2012). Although others supercritical fluids (e.g., water, ammonium, and hydrocarbons) also hold considerable promise for chemical synthesis CO_2's mild critical data, benign character, and low costs make it particularly attractive, (LEITNER, 2002).

The use of supercritical CO_2 as solvent satisfies several green chemistry and engineering principles. In contrast to most organic solvents traditionally applied as reaction media, it has low toxicity, it is nonflammable, and it is an abundantly available resource (SCURTO; HUTCHENSON; SUBRAMANIAM, 2009). A wide variety of catalytic reactions where the use of CO_2 as solvent contributes for enhancing products yields have already been reported (SKOUTA, 2009). Particularly, the levulinic acid esterification with ethanol, to our knowledge, has been the object of only one study so far.

DA SILVA JUNIOR *et al.* (2020) performed a systematic study on the esterification kinetics of levulinic acid with ethanol over the clay mineral catalyst *montmorillonite* K10. The authors investigated the effect of different process conditions with and without the addition of $scCO_2$ on the reaction kinetics. Their work

makes it clear that the levulinic acid esterification with ethanol catalyzed by *montmorillonite* K10 benefits from the addition of $scCO_2$, suggesting that the same might be true for other catalysts.

3 MATERIAL AND METHODS

This section initially introduces the materials applied for the esterification reactions, as well as the experimental apparatus and procedures. Further, the kinetic modeling strategy is presented in detail. At last, the equation of state considered and the binary interaction parameters fitting approach are described.

3.1 ESTERIFICATION REACTIONS

Levulinic acid (≥ 97 wt%, CAS number 123-76-2) was purchased from Sigma-Aldrich (São Paulo, Brazil). Ethanol (99.8 wt%, CAS number 64-17-5) was obtained from Neon (São Paulo, Brazil). Carbon dioxide (> 99 wt% liquid-phase, CAS number 124-38-9) was purchased from Air Liquide (Paraná, Brazil). Commercial Amberlyst-15 (DOW Chemical Company) with a moisture content evaluated along with the experiments of 18 ± 3 % was used as the catalyst. Typical properties for this microporous ion-exchange resin are listed in Table 1. All components (reactants, catalyst, and carbon dioxide) were used as provided by suppliers, without any additional treatment.

Table 1: Typical properties of Amberlyst-15 ion exchange resin.

Bulk density (g/L)	Hydrogen concentration (meq/g)	Surface area (m^2/g)	Average pore diameter (Å)
608	4.7	50	240

REFERENCE: (ZIYANG; HIDAJAT; RAY, 2001).

Esterification reactions were carried out in a nominal 50 mL Parr Micro Stirred Reactor (Parr Series 4590, model 4597), equipped with digital temperature and stirring speed indicators and controllers, and a pressure indicator. The nominal and the actual volume of the reactor may differ due to the instrumentation, connections, and auxiliary pipes. The actual volume of the reactor is an important variable for reactions with components above their critical temperature because all connections for instrumentation and auxiliary pipes are accessible for a light phase and will play an important role in the phase partition inside the reactor.

To measure the actual reactor volume, different quantities of CO_2 (40 g and 50 g) were fed to the reactor, using a syringe pump (Teledyne Isco model 260D) operating at constant temperature (15 °C controlled by a thermostatic bath) and pressure (150 bar). The stirring speed was set to 100 rpm and the reactor was heated from 60 °C (to allow a proper temperature control) to 100 °C in 10 °C steps. At each 10 °C step, the system's temperature was kept constant for around 30 min to reach an equilibrium condition, and the system's pressure was recorded. The CO_2 density corresponding to each of these equilibrated temperature and pressure conditions was retrieved from the literature and used to calculate an experimental reactor volume at each 10 °C step for each fed mass of CO_2. The average result for the actual reactor volume was 99 mL ± 2 mL, which was adopted in all calculations in this work.

In the experimental procedure, levulinic acid, ethanol, and Amberlyst-15 were weighted and manually loaded into the reactor. Then, with the system at room temperature, the desired amount of CO_2 was added using the syringe pump that operates at constant pressure (150 bar) and temperature (15 ºC controlled by a thermostatic bath). The stirring speed in the reactor was set to 100 rpm, which was defined based on preliminary tests.

After the reactor was loaded with all reactants, catalyst, and CO_2, its heating was initiated and the temperature and pressure profiles were recorded during all reactions. After established the desired reaction time, the reactor was cooled down, slowly depressurized (at a rate around 10 bar/min), and the content remaining in the vessel was treated as a single sample. For all experimental conditions, the levulinic acid conversion (2) was calculated based on initial (synthetic samples) and final acidity contents.

$$Conversion(\%) = \left(\frac{Initial\ Acidity\ -\ Final\ Acidity}{Initial\ Acidity} \right) \cdot 100 \qquad (2)$$

Briefly, the acidity of 0.5 g duplicated samples, diluted in ethanol, was measured by titration with a standardized 0.05 mol/L solution of sodium hydroxide.

3.2 KINETIC MODELING

The differential mole balance inside the reactor might be written, in terms of levulinic acid conversion (X_{LA}), as follows (equation (3)),

$$\frac{dX_{LA}}{dt} = \rho_c \frac{(-r_{LA})}{n_{LA0}} \tag{3}$$

where n_{LA0} is the initial mol number of levulinic acid, t is time, and ρ_c is the catalyst mass concentration (mass per volume) in the liquid phase. If the system is homogeneous, then ρ_c is the mass concentration in the single fluid phase. At this point, it is worth mentioning that the reaction rate, r_{LA}, is a function of temperature and phase partition, but neither is constant in the reaction set up here presented. Thus, a non-isothermal approach was followed to compute the temperature profiles, and *v-T* flash calculations were performed to handle the phase partition inside the reactor vessel at each integration step while solving the differential mole balance. Both, the non-isothermal approach, as well as the *v-T* flash calculations, are further described.

In this work, the reaction rate is represented using an activity-based Langmuir-Hinshelwood rate law, considering that the surface reaction is the rate-controlling step (equation (4)), as follows (HAMERSKI *et al.*, 2020).

$$\begin{aligned}
(-r_{LA}) &= \frac{k\left(a_{LA}a_{EtOH} - \frac{1}{K_{eq}}a_{EL}a_{W}\right)}{(1 + K_{ads,LA}a_{LA} + K_{ads,EtOH}a_{EtOH} + K_{ads,EL}a_{EL} + K_{ads,W}a_{W})^2} \\
k &= k^o \exp\left[-Ea/R\left(T^{-1} - 383.15^{-1}\right)\right] \\
K_{eq} &= {K_{eq}}^o \exp\left[\Delta H_R/R\left(383.15^{-1} - T^{-1}\right)\right]
\end{aligned} \tag{4}$$

where k^o and ${K_{eq}}^o$ are the kinetic and equilibrium constants at a reference temperature, Ea is the activation energy, R is the universal gas constant, T is the temperature, ΔH_r is the reaction enthalpy, which is assumed as constant in this

formulation, $K_{ads,i}$ is the adsorption constant of each i component, and a_i is the activity of each i product or reactant. In an isofugacity approach (ϕ-ϕ), the activity of a given component in a mixture in a specific phase is defined as (equation (5)).

$$a_i = x_i \gamma_i = x_i \frac{\hat{\phi}_i}{\phi_i} \tag{5}$$

where x_i and γ_i are the mole fraction and activity coefficient of a certain component, respectively, and $\hat{\phi}_i$ and ϕ_i are the fugacity coefficients of a component in a mixture and as a pure component at the same temperature and pressure.

A reference temperature (see equation (4)) was adopted for Arrhenius's equation to dimmish the correlation between the parameters k and Ea (SCHWAAB; PINTO, 2007). In this work, 383.15 K was adopted as the reference temperature for both Arrhenius's and Van't Hoff's equations because it is the setpoint temperature of most kinetic data and thus should provide a low correlation factor.

To correlate the kinetic model to experimental data, the parameters (k^o, $K_{eq}{}^o$, Ea, ΔH_r, and $K_{ads,i}$'s) were pre-estimated using the stochastic particle swarm optimization (PSO) algorithm and refined using the Nelder−Mead Simplex method from Matlab's optimization toolbox. Equations (6) and (7) were the objective function and the correlation criteria applied in this work for the estimation of the kinetic parameters.

$$OF = \sum_{j=1}^{n} \left(X_{exp,j} - X_{calc,j} \right)^2 \tag{6}$$

$$RMSD = \sqrt{\frac{\sum_{j=1}^{n} \left(X_{exp,j} - X_{calc,j} \right)^2}{n}} \tag{7}$$

3.2.1 Non-isothermal reaction approach

For all kinetic experiments, the reactants and the catalyst were loaded into the reactor at room temperature. The heating of the reactant mixture to the

temperature setpoint is a dynamic process and takes considerable time depending on the reactor heating system. The reactor used in this study took around 6 minutes to reach the temperature setpoint for the reactions hereby considered. Therefore, as the levulinic acid esterification with ethanol in this reaction set-up presents considerably high reaction rates, a non-isothermal approach was considered in this study. Based on preliminary tests, it was found out that even with the highest catalyst loadings, the conversion of levulinic acid from the initial instant that the heating system was turned on to the moment that the reactor reaches 45 °C is negligible. Hence, the instant that the reactor reaches 45 °C was taken as zero reaction time in all non-isothermal kinetic experiments.

The final reaction time, on the other hand, was taken as the moment that the reactor starts to cool down. The cooling down was not considered as reaction time because it is considerably faster than the heating up. Besides, by neglecting it, we could assume the same temperature profile for all reaction runs at the same kinetic set, avoiding extra computational time in the simulations (kinetic calculations coupled to *v*-*T* flash).

As mentioned in Section 3.1, each experiment in a kinetic set is destructive, meaning that each reaction experiment (each circle in Figure 2) has its own temperature profile (each colored line in Figure 2). Thus, to include the heating ramp in the kinetic modeling, it was defined a function $T(t)$, inherent to each kinetic set, such that $T(t)$ is equal to the average of the temperature profiles of all runs up to the temperature setpoint, and later $T(t)$ is equal the temperature set point. Figure 2 exemplifies how we are treating the kinetic data.

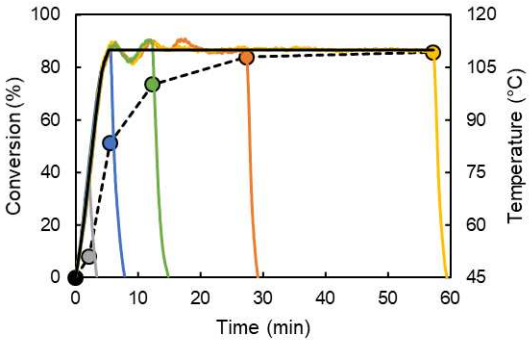

Figure 2: Example of conversion and temperature profiles for a kinetic set. The continuous black line represents the $T(t)$ inputted for the kinetic modeling, the continuous colored lines are the recorded temperature profile at each reaction run, and the colored circles are the corresponding levulinic acid conversions with a dashed line as a guide to the eye.

3.2.2 *v-T* flash

As mentioned before, the use of $scCO_2$ might promote phase partition inside the reactor. Thus, to compute the reaction rate, while solving the differential material balance (equation (3)), *v-T* flash calculations are required at each integration time step.

A *v-T* flash problem consists in finding the system's pressure (P), the vaporized fraction (β), the molar volumes of the liquid (v_L) and vapor (v_V) phases, and the molar fractions of the liquid ($\boldsymbol{x}$) and vapor ($\boldsymbol{y}$); given that the system is in equilibrium, its global molar volume (v), its temperature (T), and its overall molar fraction ($\boldsymbol{z}$).

In this work, the *v-T* flash procedure proposed by Cismond et al. (2018) was used. In a *v-T* flash problem, to guarantee the equilibrium, temperature, pressure, and fugacity of each (i) component in each phase must be the same. Besides, the global material balance and the material balance by component must be satisfied. Additionally, the sum of the liquid and vapor phase volumes must be the volume of the system. These conditions, in a $\boldsymbol{\phi}$-$\boldsymbol{\phi}$ approach for a system of C components, can be written as follows in equations (7) to (11).

$$\hat{\phi}_i^L x_i = \hat{\phi}_i^V y_i \quad \text{(fugacity equality; } i = 1, 2, ..., C \text{)} \tag{8}$$

$$y_i\beta + x_i(1-\beta) = z_i \quad \text{(component material balance; } i = 1,2,...,C\text{)} \tag{9}$$

$$\sum_{i=1}^{C} x_i = \sum_{i=1}^{C} y_i = 1 \quad \text{(global material balance)} \tag{10}$$

$$P(\boldsymbol{x}, T, v^L) = P(\boldsymbol{y}, T, v^V) \quad \text{(pressure equality)} \tag{11}$$

$$v^L(1-\beta) + v^V\beta = v \quad \text{(volume distribution)} \tag{12}$$

At this point, it is convenient to rearrange some equations in terms of the component's *K*-values (equation (13)). By doing so, equation (8) becomes equation (14), and equation (10) becomes the Rachford-Rice equation (15). Finally, for a set of *K*-values, equation (15) can be solved for β and the mole fractions in the liquid and vapor phases are obtained from equations (16) and (13) respectively.

$$y_i = K_i x_i \quad (i = 1,2,...,C) \tag{13}$$

$$\ln K_i - \ln \hat{\phi}_i^L + \ln \hat{\phi}_i^V = 0 \quad (i = 1,2,...,C) \tag{14}$$

$$\sum_{i=1}^{C} \frac{z_i(K_i - 1)}{1 - \beta + \beta K_i} = 0 \quad (i = 1,2,...,C) \tag{15}$$

$$x_i = \frac{z_i}{1 - \beta + \beta K_i} \quad (i = 1,2,...,C) \tag{16}$$

The algorithm proposed by Cismondi et al.(2018) is summarized in Figure 3. Their strategy is based on a *P-T* flash with successive substitution to converge the *K*-values, as proposed by Michelsen (MICHELSEN, 1982). However, since there is no pressure specification in a *v-T* flash problem, at each outer successive substitution loop, the pressure equality (11) and the volume distribution (12) must be satisfied.

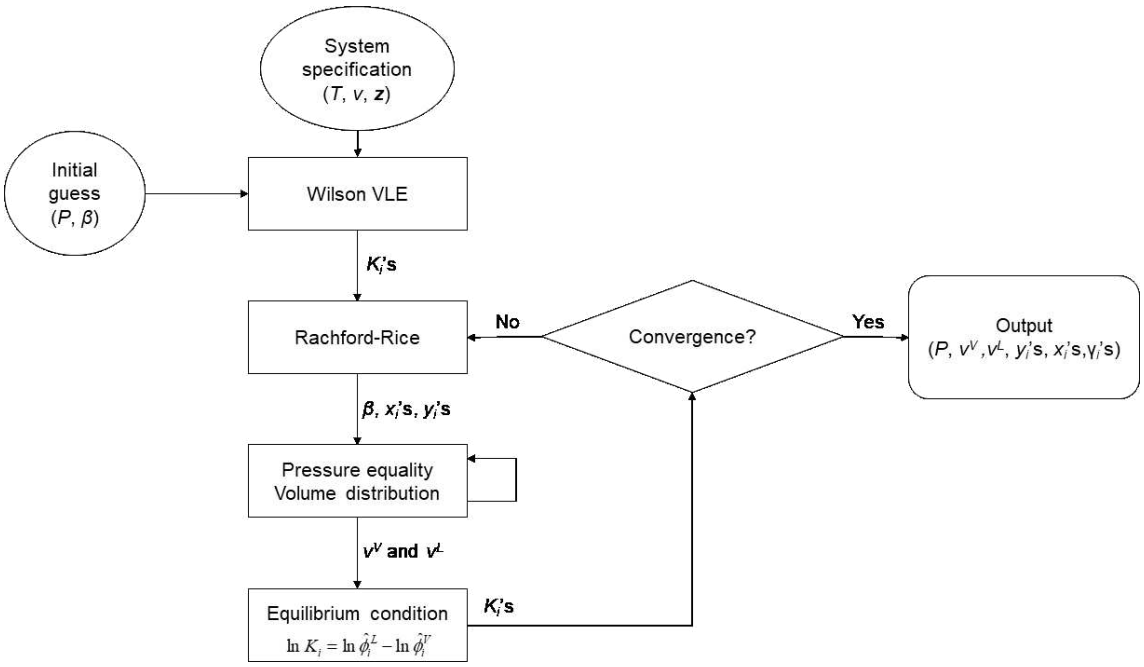

Figure 3: *v-T* flash algorithm, based on Cismondi et al. (2018).

Therefore, v_V is written in terms of v_L. Then, equation (12) becomes equation (17), and equation (11) becomes the single variable equation (19) that is solved with Newton's iteration using their derivatives (equations (18) and (20)). Cismondi et al. (2018) suggest 1.5 times the mixture co-volume as an initial guess for v_L. In the present work, however, we adopted 2 times the mixture co-volume which performed better for the system studied.

$$v^V = \frac{v-(1-\beta)v^L}{\beta} \tag{17}$$

$$\frac{\partial v^V}{\partial v^L} = -\frac{(1-\beta)}{\beta} \tag{18}$$

$$F = P(\boldsymbol{y},T,v^V) - P(\boldsymbol{x},T,v^L) = 0 \tag{19}$$

$$\frac{\partial F}{\partial v^L} = \frac{\partial P(\boldsymbol{y},T,v^V)}{\partial v^V}\frac{\partial v^V}{\partial v^L} - \frac{\partial P(\boldsymbol{x},T,v^L)}{\partial v^L} \tag{20}$$

For each kinetic condition, the algorithm was initialized according to Figure 2. So, it was taken as initial guesses: the experimental pressure for P, 0.5 for β, and the Wilson VLE (equation (21)) for the K_i's. Later, for all the other time steps in the

same kinetic set, the algorithm was initialized with the previous converged values of P, β, and K_i's to improve the convergence rate and avoid extra computational time.

$$K_i = \frac{P_{ci}}{P}\exp\left[5.373\left(1+\omega_i\right)\left(1-\frac{T_{ci}}{T}\right)\right] \tag{21}$$

3.3 PHASE-EQUILIBRIUM MODELING

A *v-T* flash algorithm is computationally expensive, even more, when coupled in the solution of a differential equation, as in this case. Thus, to describe the thermodynamic behavior of the reaction system, the Peng-Robinson equation of state (PENG; ROBINSON, 1976) with the conventional quadratic van der Waals mixing rule (equation (22)), and the Boston-Mathias alpha function (equation (23)) (MATHIAS, 1983) was selected. The Peng-Robinson equation of state was chosen because, besides its industrial appealing, it offers a good balance between an accurate description for systems involving one supercritical component at medium and high pressures and a fast computational processing (LOPEZ-ECHEVERRY; REIF-ACHERMAN; ARAUJO-LOPEZ, 2017).

$$\begin{aligned}
P &= \frac{RT}{v-b} - \frac{\mathrm{a}(T)}{v(v+b)+b(b-v)} \\
\mathrm{a}(T) &= \sum_{i=1}^{n}\sum_{j=1}^{n} x_i x_j \sqrt{\mathrm{a}_i(T)\mathrm{a}_j(T)}\,(1-k_{ij}) \\
b &= \sum_{i=1}^{n}\sum_{j=1}^{n} x_i x_j\, 0.5(b_i+b_j)(1-l_{ij}) \\
b_i &= 0.07780\frac{RT_{ci}}{P_{ci}} \\
\mathrm{a}_i(T) &= 0.45724\frac{R^2 {T_{ci}}^2}{P_{ci}}\alpha_i(T)
\end{aligned} \tag{22}$$

$$\alpha_i(T)^{0.5} = \begin{cases} 1 + m_i\left[1 - \left(\dfrac{T}{T_{ci}}\right)^{0.5}\right]^2 & \text{if } T < T_{ci} \\ \exp\left\{\dfrac{2+m_i}{2}\left[1 - \left(\dfrac{T}{T_{ci}}\right)^{\frac{m_i}{2+m_i}}\right]\right\} & \text{else} \end{cases} \qquad (23)$$

$$m_i = 0.37464 + 1.54226\omega_i - 0.26992\omega_i^2$$

To improve the multicomponent VLE representation, isothermal binary phase-equilibrium data for some pairs of components in the system of interest in this study (CO_2, reactants, and products) were correlated with the cubic equation of state. The saturation points calculations were performed according to the procedure proposed by Michelsen (MICHELSEN, 1985) and the binary interaction parameters k_{ij} and l_{ij} were adjusted using the Nelder−Mead Simplex method from Matlab's optimization toolbox to minimize the least-squares function (equation (24)), and the root mean square deviation ($RMSD$) (equation (25)) was considered as the statistical criteria for the parameter estimation.

$$OF = \sum_{j=1}^{n}\left(P_{exp,j} - P_{calc,j}\right)^2 \qquad (24)$$

$$RMSD = \sqrt{\frac{\sum_{j=1}^{n}\left(P_{exp,j} - P_{calc,j}\right)^2}{n}} \qquad (25)$$

To handle *P-x* data, only the bubble points were considered for the objective function (equation (24)), and both bubble and dew points were included in the $RMSD$ calculation. When dealing with *P-xy* data, only the saturated liquid phase composition (bubble points) was considered for $RMSD$ calculations.

The critical properties of the pure components used in this study are presented in Table 2.

Table 2: Critical properties of the pure components used in this study.

Component	T_c (K)	P_c (bar)	ω	Reference
Levulinic acid	738.0	40.20	0.75575	Aspen Plus databank
Ethanol	514.0	61.37	0.64355	DIPPR801
Ethyl levulinate	666.1	29.24	0.60709	Aspen Plus databank
Water	647.1	220.64	0.34486	DIPPR801
CO_2	304.2	73.83	0.22362	DIPPR801

4 RESULTS AND DISCUSSION

In this study, to make the most of the capability of the thermodynamic model to represent the non-ideality of the multicomponent system studied, binary interaction parameters were fitted using vapor-liquid equilibrium data of some binary systems involved in the levulinic acid ethanolic esterification assisted by $scCO_2$. Therefore, initially, are presented the results of the binary interaction parameters (k_{ij} and l_{ij}) fitting performed in this work. Later on, the results regarding the experimental kinetics and the kinetic modeling are introduced and discussed.

4.1 BINARY INTERACTION PARAMETERS DETERMINATION

Binary phase-equilibrium data of the components in the system, in a temperature and pressure range as close as possible to the reaction conditions, was retrieved from the literature and correlated with the Peng-Robinson equation of state with the van der Waals quadratic mixing rule and the Boston Mathias alpha function, as described in Section 3.3. Table 3 summarizes the databank considered, the fitted binary interaction parameters, and the corresponding $RMSD$.

Table 3: Summary of the fitted binary interaction parameter for each binary pair considered.

System [Type of data]	Isotherms (°C) [Reference]	Fitted binary interaction parameters	*RMSD* (bar)
CO_2 + levulinic acid [*P-x* data]	30, 40, 50, 60, 70, 80 [a]	$k_{ij} = -0.02560 + 1.780 \cdot 10^{-4} T$ $l_{ij} = 0.01658 - 6.436 \cdot 10^{-5} T$	5.72
CO_2 + ethyl levulinate [*P-x* data]	30, 40, 50, 60, 70, 80 [a]	$k_{ij} = 0.003088$ $l_{ij} = -0.03759$	4.77
CO_2 + ethanol [*P-xy* data]	40, 60 [b]; 80 [c]; 100 [d]; 118.8 [e]	$k_{ij} = 0.08006$ $l_{ij} = -0.03493$	2.41
CO_2 + water [*P-xy* data]	50, 75, 100, 125 [f]	$k_{ij} = 0.02450 - 6.201 \cdot 10^{-4} T$ $l_{ij} = 0.4126 - 6.282 \cdot 10^{-4} T$	2.58
		$^{(*)} k_{ij} = 0.2749 - 2.885 \cdot 10^{-5} T$ $l_{ij} = 0.4126 - 6.282 \cdot 10^{-4} T$	18.45
Ethanol + water [*P-xy* data]	50, 70, 90 [g]; 108.2, 130.4, 150.6 [h]; 200, 250, 275, 300 [i]	$k_{ij} = 0.03682$ $l_{ij} = 0.1284$	0.41

[a] - GIACOMIN JUNIOR *et al.*, 2019.

[b] - SUZUKI *et al.*, 1990.

[c] - SECUIANU; FEROIU; GEANĂ, 2008.

[d] - GALICIA-LUNA; ORTEGA-RODRIGUEZ; RICHON, 2000.

[e] - DE LA CRUZ; GALICIA-LUNA, 1999.

[f] - HOU; MAITLAND; TRUSLER, 2013.

[g] - KOLBE; GMEHLING, 1985.

[h] - CRISTINO *et al.*, 2013.

[i] - BARR-DAVID; DODGE, 1959.

(*) - Binary interaction parameters fitted with equation (25) as the objective function.

To our knowledge, there is no VLE data for the system ethyl levulinate + levulinic acid. Resk et al. (RESK *et al.*, 2014) reported single sets of low temperature (60 °C) for the systems ethanol + levulinic, ethanol + ethyl levulinate, water + levulinic acid, which resulted in saturation pressures lower than 0.5 bar. Since their data is far from our temperature/pressure reaction conditions, binary interaction parameters for these systems were not fitted, to avoid overfitting their VLE to conditions far from our interest.

Figures Figure 4 to Figure 8 show the experimental data from the literature for each binary system as well as the VLE calculation using zero as binary interaction parameters and the optimized values presented in Table 3.

Among the studied systems, CO_2 + ethyl levulinate was the only one for which a good qualitative description was observed without binary interaction parameters. Compounds with carbonyl groups are known to have a good affinity for CO_2 (RAVEENDRAN; IKUSHIMA; WALLEN, 2005). Ethyl levulinate presents two carbonyl groups in its structure and follows this trend, presenting the highest CO_2 absorption capacity among biobased solvents with a similar structure (DENG *et al.*, 2015). This might be the reason why a more ideal-like behavior is observed for the liquid phase of this system. To obtain an accurate description at the higher temperatures and to predict the dew points, temperature-independent binary interaction parameters were fitted (Figure 4 (B)).

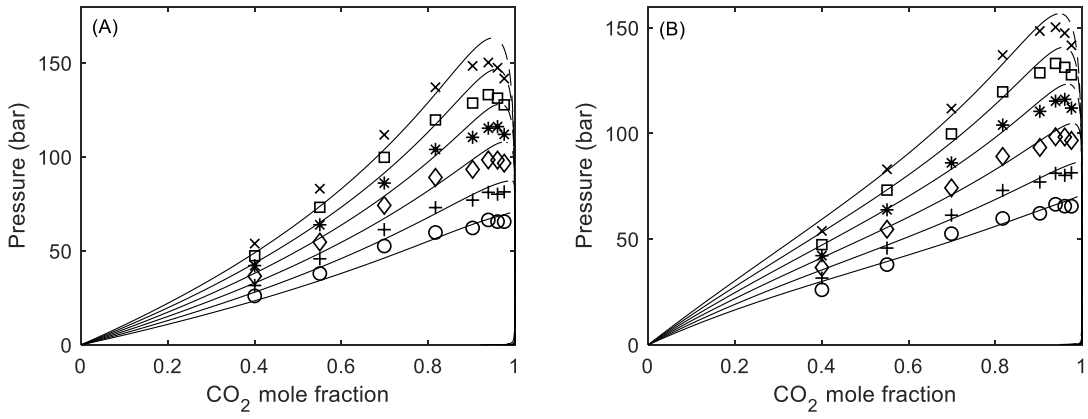

Figure 4: Experimental and calculated VLE for the system CO_2 + ethyl levulinate at 30 °C (○), 40 °C (+), 50 °C (◊), 60 °C (*), 70 °C (□) and 80 °C (×) with the Peng-Robinson equation of state with Boston Mathias alpha function setting the binary interaction parameters to zero (A), and to the optimized values from Table 3 (B).

Levulinic acid, ethanol, and water are associative compounds that are subjected to strong short-ranged interactions (hydrogen bonding). Although carbon dioxide has been historically treated as a nonpolar molecule, due to its low dielectric constant and zero dipole moment, its significant quadrupole moment provides unique features in the presence of polar compounds, such as its capacity of participating in hydrogen bonding interactions (RAVEENDRAN; IKUSHIMA; WALLEN, 2005). Thus, it is not surprising that the Peng Robinson equation of state with Boston Mathias

alpha function, which does not account for such phenomena, failed to predict the phase behavior of these compounds (levulinic acid, ethanol, and water) with CO_2 when the binary interaction parameters were set to zero.

Aiming for a better description, binary interaction parameters were fitted for these systems. For CO_2 + ethanol, temperature-independent parameters were sufficient to obtain a low $RMSD$ (Table 3) and a good prediction of the vapor phase composition at the bubble points (Figure 5). For CO_2 + levulinic acid, as presented in Figure 6, temperature-dependent parameters were needed to effectively correlate the bubble pressures and predict the dew points. It is worth pointing out that the shape of the pressure composition for this system might suggest LLV behavior, however, the authors that reported the experimental data (GIACOMIN JUNIOR *et al.*, 2019) mentioned that they did not observe these three-phase transitions experimentally.

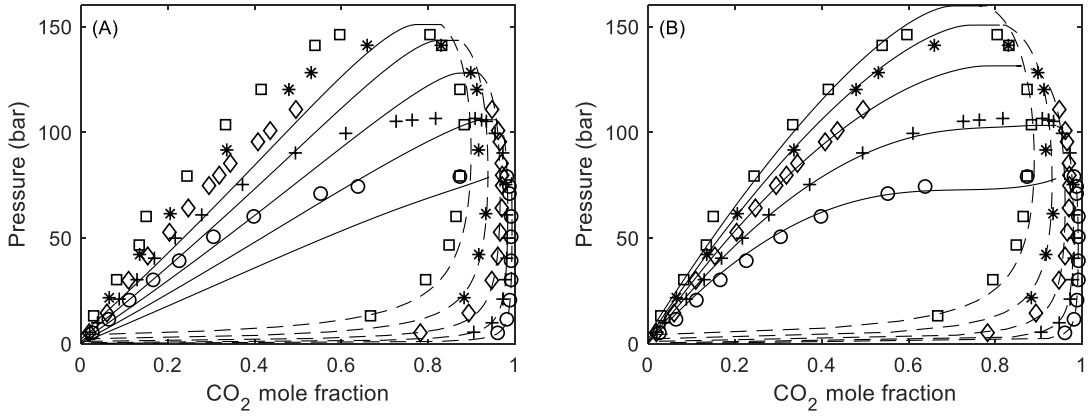

Figure 5: Experimental and calculated VLE for the system CO_2 + ethanol at 40 °C (○), 60 °C (+), 80 °C (◊), 100 °C (*), and 118.81 °C (□) with the Peng-Robinson equation of state with Boston Mathias alpha function setting the binary interaction parameters to zero (A), and to the optimized values from Table 3 (B).

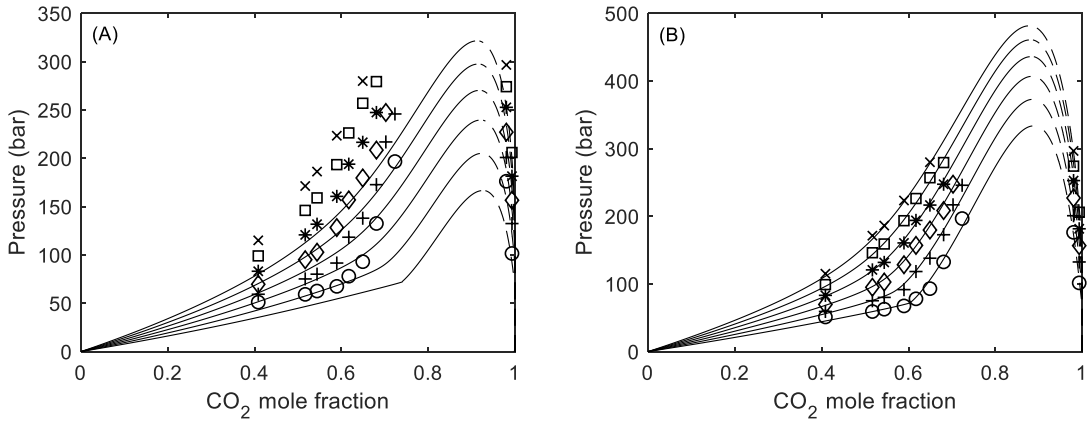

Figure 6: Experimental and calculated VLE for the system CO_2 + levulinic acid at 30 °C (○), 40 °C (+), 50 °C (◊), 60 °C (*), 70 °C (□) and 80 °C (×) with the Peng-Robinson equation of state with Boston Mathias alpha function setting the binary interaction parameters to zero (A) and to the optimized values from Table 3 (B).

The system CO_2 + water shows a type III phase behavior according to Scott and Konyenenburg classification (KONYNENBURG; SCOTT, 1980). It presents two critical lines. One that extends from the critical point of water, presumably terminating at the melting curve, and another that extends from the critical point of CO_2 to an upper critical endpoint (UCEP) (SHYU *et al.*, 1997). For this system, fitting temperature-dependent binary interaction parameters by minimizing equation (24) provided a low $RMSD$, however, a drastic difference between the calculated and the experimental vapor phase composition at the bubble points is observed (see Figure 7 (B)).

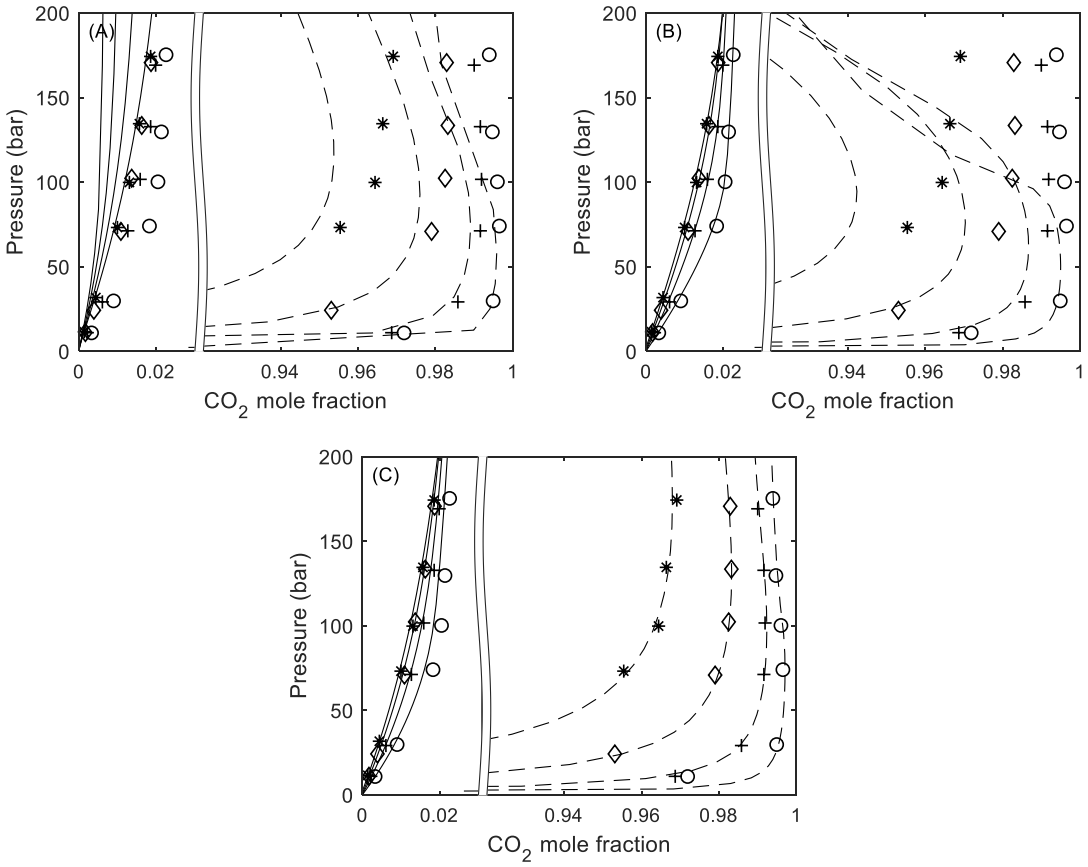

Figure 7: Experimental and calculated VLE for the system CO_2 + water at 50 °C (○), 75 °C (+), 100 °C (◊), 125 °C (*) with the Peng-Robinson equation of state with Boston Mathias alpha function setting the binary interaction parameters to zero (A) and to the optimized values from Table 3 (B and C).

Water is a highly polar and associative molecule that presents an extremely low affinity for CO_2. Even statistical mechanics-based equations of state that explicitly account for such associating interactions struggle to accurately represent the CO_2 + water phase behavior (DIAMANTONIS; ECONOMOU, 2012; MONTEIRO; PEREIRA, 2020). Thus, it is not surprising that a traditional cubic equation of state with a classic mixing rule would fail in representing the phase behavior of this system. Attempting to enhance the description of the vapor phase composition and the overall representation of CO_2 + water phase behavior, another set of binary interaction parameters was obtained with a different objective function, equation (26), that also contemplates the vapor phase composition at the bubble points.

$$OF = \sum_{j=1}^{n} \left\{ \frac{\left[\left(P_{exp,j} - P_{calc,j} \right) / P_{exp,j} \right] \left(y_{exp,j} - y_{calc,j} \right)}{\sqrt{\left[\left(P_{exp,j} - P_{calc,j} \right) / P_{exp,j} \right]^2 + \left(y_{exp,j} - y_{calc,j} \right)^2}} \right\}^2 \quad (26)$$

As can be seen from Figure 7(C), the general description of the CO_2 + water phase behavior seems more coherent with this new set of binary interaction parameters. Therefore, despite the high $RMSD$ as reported in Table 3, we recommend this set of binary interaction parameters for the temperature range from 50 °C to 125 °C and adopted them in the kinetic modeling.

Finally, as depicted in Figure 8, the cubic equation of state also failed to predict the ethanol + water VLE behavior, when considering the binary interaction parameters set to zero (Figure 8 A, C, and E). However, a single set of temperature-independent binary interaction parameters provided a surprisingly good description over a wide range of temperatures (from 50 to 300 °C) and saturation pressures (from 0.1 to 125 bar) that covers most reaction conditions in the present study.

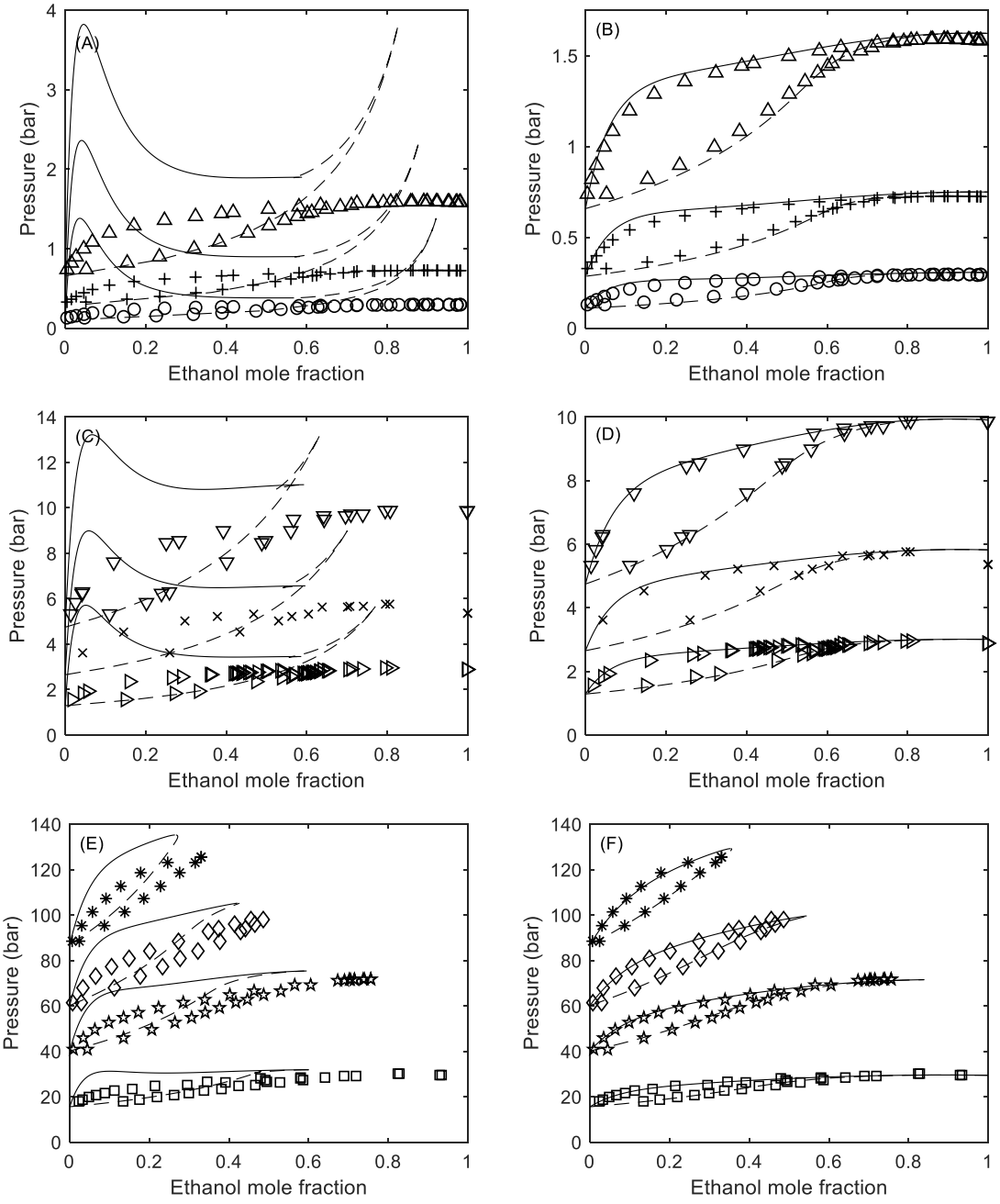

Figure 8: Experimental and calculated VLE for the system ethanol + water at 50 °C (○), 70 °C (+), 90 °C (△), 108.2 °C (▷), 130.35 (×), 150.55 (▽), 200 (□), 250 (☆), 275 (◊), and 300 (*) with the Peng-Robinson equation of state with Boston Mathias alpha function setting the binary interaction parameters to zero (A, C and E) and to the optimized values from Table 3 (B, D, and F).

Overall, the Peng-Robinson equation of state with Boston Mathias alpha function and a classic quadratic mixing rule provided a good VLE description of the binary systems considered in this section when using the binary interaction parameters reported in Table 3. Unfortunately, due to the lack of VLE data in a

temperature-pressure range close to the reaction conditions, the binary pairs not contemplated in Table 3, were not evaluated and had their binary interaction parameters set to zero.

4.2 EXPERIMENTAL KINETICS AND MODELING

Kinetics of levulinic acid esterification with ethanol, catalyzed by Amberlyst-15 and in a $scCO_2$-assisted scheme were accessed in several process conditions, varying temperature, ethanol to levulinic acid molar ratio, catalyst, and CO_2 loads. Table 4 summarizes the process variables adopted at each experimental kinetic set as well as corresponding levulinic acid conversion obtained at the largest reaction time evaluated.

Table 4: Process conditions and the corresponding levulinic acid conversion at the longest run at each experimental kinetic set.

Kinetic set	Molar ratio [a]	Catalyst load [b] (wt%)	Temperature [c] (°C)	CO_2 load [d]	Conversion [e] (%)
K1*	1:1	5	110	3:1	65.6
K2	3:1	5	110	3:1	85.8
K3	6:1	5	110	3:1	90.6
K4*	9:1	5	110	3:1	94.0
K5*	6:1	2	110	3:1	91.1
K6	6:1	10	110	3:1	90.9
K7	6:1	10	100	3:1	91.6
K8	6:1	10	90	3:1	91.4
K9*	6:1	10	80	3:1	88.0
K10	6:1	10	110	1:1	90.3
K11	6:1	10	110	5:1	95.6

[a] - Ethanol to levulinic acid molar ratio

[b] - Expressed as weight of catalyst divided by weight of levulinic acid (%)

[c] - Temperature set point (°C)

[d] - Expressed as CO_2 to reagents weight ratio

[e] - Levulinic acid conversion.

Only the conditions marked with an asterisk (*) in Table 4 were selected for the kinetic parameters fitting to verify the predictive capacity of the kinetic model. These conditions were chosen to cover the maximum and minimum values accessed for each process variable except for the CO_2 load, which is further discussed.

The reaction equilibrium constant, as a thermodynamic property is defined according to equation (27),

$$K_{eq} = K_x K_\gamma = \left(\frac{x_{EL} x_W}{x_{LA} x_{EtOH}} \right)_{eq} \left(\frac{\gamma_{EL} \gamma_W}{\gamma_{LA} \gamma_{EtOH}} \right)_{eq} = \left(\frac{a_{EL} a_W}{a_{LA} a_{EtOH}} \right)_{eq} \quad (27)$$

where the subscript "$_{eq}$" means that the quantities must be in equilibrium, i.e., the value of each variable inside the parenthesis must correspond to its value at the equilibrium levulinic acid conversion.

The trend of the experimental kinetic data (see Figure 10) reveals that the levulinic acid conversions reported in Table 4 are close to the equilibrium conversions for the different molar ratios. Initial parameter fitting attempts with a mole fraction-based rate law (γ_i's = 1) were unsuccessful to match these near-equilibrium conversions. It seems that the highly associative character of the main components and the high-pressure condition of the system confers a strong non-ideality to the reactional mixture. Thus, it is concluded that an activity-based rate law must be used to consider the correct interaction for this multicomponent system.

However, even the parameter fitting considering a standard activity-based rate law (equation (4)) was also unsuccessful to match the near-equilibrium conversions at different molar ratios. To further investigate this, experimental equilibrium constants, from equation (27), were calculated for each molar ratio, assuming that the conditions K1, K2, K3, and K4, reported in Table 4, reached their equilibrium conversion. Table 5 shows these results.

Table 5: Experimental equilibrium constants for the different molar ratios assuming that these conditions reached their equilibrium conversions.

Kinetic set	Molar ratio	Conversion (%)	K_x	K_{eq}
K1	1	65.61	3.50	10.97
K2	3	85.80	2.29	5.87
K3	6	90.63	1.75	4.54
K4	9	93.93	1.63	4.03

As shown in Table 5, different molar ratios lead to different calculated equilibrium constants, which is not thermodynamically consistent. Either due to inherent limitations of a cubic equation of state or due to the lack of binary interaction parameters for the mixtures not contemplated in Table 3, the Peng Robinson equation of state with Boston Mathias alpha function and a classic quadratic mixing rule fails on the estimate of the activity coefficients for this system.

Thus, in the pursuit of a better representation of the kinetic data, we adopted an empirical strategy to allow the kinetic model to match the equilibrium conversion for different molar ratios. As shown in Figure 9, the values of the experimental equilibrium constant from Table 5 have an exponential dependence with the initial levulinic acid mole fraction on a CO_2-free basis, which can be defined, in terms of the ethanol to levulinic acid molar ratio (MR), as $z_{LA}^* = 1/(1+MR)$.

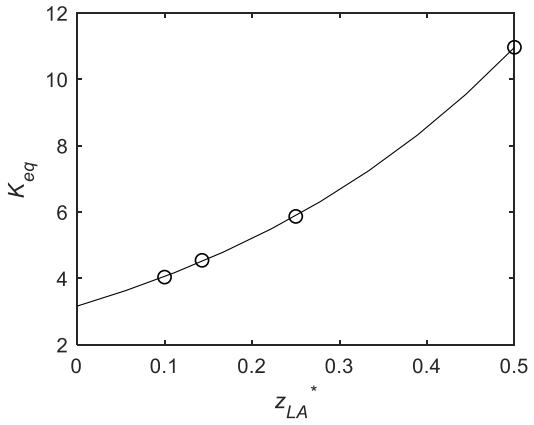

Figure 9: Exponential dependence of the experimental equilibrium constants from Table 5 with the initial levulinic acid mole fraction on a CO_2-free basis.

Therefore, in the rate equation (equation (4)), the equilibrium constant at the reference temperature was redefined as $K_{eq}{}^{o} = K_{eq}{}^{*} \exp(\lambda z_{LA}{}^{*})$, adding one extra adjustable parameter (λ) to the kinetic model. This empirical approach led to a good correlation, as presented in Table 6, where the results of the fitted parameters and the corresponding $RMSD$ are reported.

Table 6: Kinetic parameters for the levulinic acid ethanolic esterification catalyzed by Amberlyst-15 and assisted by $scCO_2$ fitted to match the conditions marked with an asterisk from Table 4.

k^{o} (*mLmol/g/min*)	Ea (*kJ/mol*)	$K_{eq}{}^{*}$	ΔH_R (*kJ/mol*)	λ	$K_{ads,EtOH}$	$K_{ads,W}$	$RMSD$ (%)
56.09	35.94	3.21	-20.63	2.46	5.63	4.34	3.99 [a] 4.77 [b]

[a] - Considering only the conditions used for parameter fitting.

[b] - Considering all kinetic sets from Table 4.

The Langmuir-Hinshelwood mechanism considered in this work assumes three reaction steps: adsorption, surface reaction, and desorption. First molecules of the reactants (levulinic acid and ethanol) molecularly adsorb on adjacent sites. Then, the adsorbed molecules undergo a surface reaction, which is the rate-controlling step and originates the products (ethyl levulinate and water). At last, there is the desorption of the products from the catalytic sites. Adsorption parameters were considered only for ethanol and water because considering it for the other components did not improve the system's description and did not lead to better modeling results. This finding suggests that ethanol and water, the most polar molecules, are strongly adsorbed in the catalytic sites, while levulinic acid, ethyl levulinate, and CO_2 would be weakly adsorbed.

Figure 10(A) and (B) depict the simulation results for different ethanol to levulinic acid molar ratios. It is clear from the results that the empirical approach performed satisfactorily, offering a good description even for conditions different than those used for the parameter estimation. As expected, it can be seen that keeping fixed the temperature setpoint and the $scCO_2$ load, the larger is the molar ratio, the higher is the equilibrium conversion. Finally, one can observe that the reaction rates at the lower molar ratios are slightly faster. However, it must be emphasized that this is more likely a consequence of the greater absolute quantity of catalyst fed to the

system to keep the catalyst to levulinic acid mass proportion than an effect from the molar ratio itself.

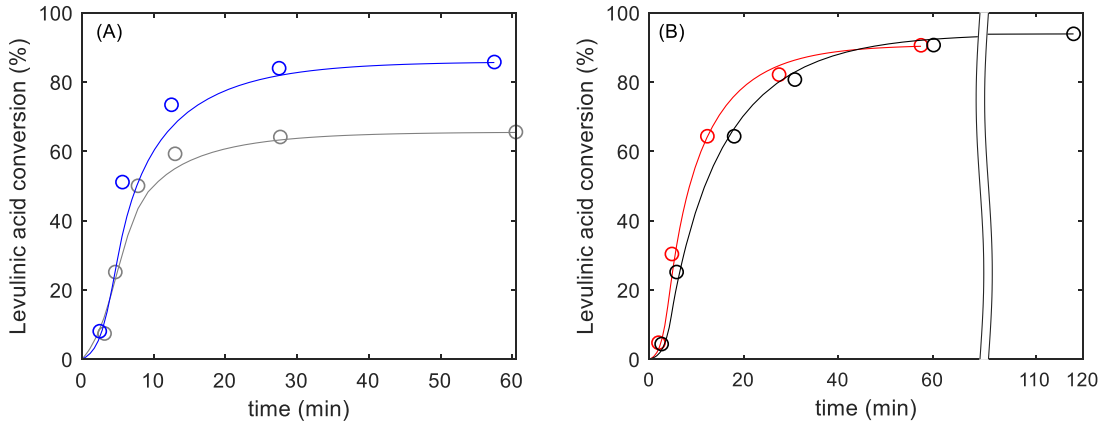

Figure 10: Experimental (circles) and simulation (continuous lines) kinetic results at different ethanol to levulinic acid molar ratios, keeping fixed the setpoint temperature (110 °C), the catalyst to acid mass relation (5 wt%) and the CO_2 to reactants mass ratio (3:1). The gray and blue colors (A) stand for ethanol to levulinic acid molar ratio of 1:1 and 3:1, respectively; and red and black colors stand for 6:1 and 9:1, respectively.

The experimental and simulated kinetics of reaction using different catalyst amounts fed to the reactor, keeping fixed the other process conditions are showed in Figure 11. An excellent agreement between the simulations and the experimental data can be observed. It also should be remarked that this reaction scheme delivered appreciable levulinic acid conversions in short reaction times, even with very low catalyst loadings.

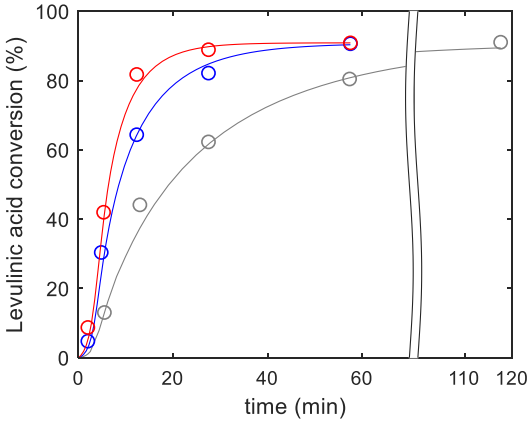

Figure 11: Experimental (circles) and simulation (continuous lines) kinetic results at different catalyst to acid mass relations, at fixed temperature setpoint (110 °C), ethanol to levulinic acid molar ratio of 6:1, and the CO_2 to reactants mass ratio of 3:1. The gray, blue, and red colors stand for 2 wt%, 5 wt%, and 10 wt% respectively.

Figure 12 depicts the simulation and experimental results when using different temperature setpoints. The model description in the setpoint temperature range from 80 °C to 110 °C is fairly good. Also, it can be seen that while little difference is observed in the equilibrium conversions, the reaction rates are fairly sensitive to the temperature set-point.

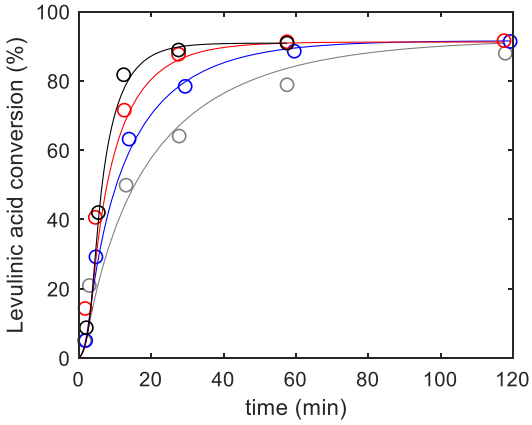

Figure 12: Experimental (circles) and simulation (continuous lines) kinetic results at different setpoint temperatures, keeping fixed the ethanol to levulinic acid molar ratio (6:1), the catalyst to acid mass relation (5 wt%), and the CO_2 to reactants mass ratio (3:1). The gray, blue, red, and black colors stand for 80 °C, 90 °C, 100 °C, and 110 °C respectively.

The CO_2 load effect in the reaction kinetics is shown in Figure 12. It must be emphasized that any CO_2 to reactants mass ratio other than 3:1 has been

considered for parameter fitting. The kinetic model offered a good prediction at 1:1 mass ratio, with little difference in the initial reaction rates, and a slightly lower equilibrium conversion, which is in agreement with the experimental data obtained.

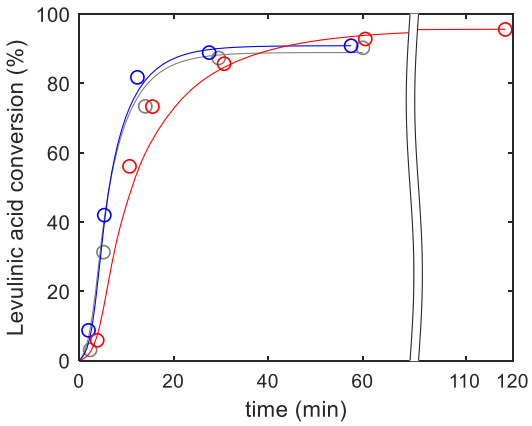

Figure 13: Experimental (circles) and simulation (continuous lines) kinetic results at different CO_2 to reactants mass ratios, keeping fixed the ethanol to levulinic acid molar ratio (6:1), the catalyst to acid mass relation (10 wt%), and the temperature setpoint (110 °C). The gray, blue, and red colors stand for 1:1, 3:1, and 5:1 CO_2 load.

Figure 12 also shows the results for the condition K11, at 5:1 CO_2 to reactants mass ratio. Due to the high amount of CO_2 in the system at this reaction condition, the reaction mixture is outside the predicted two-phase envelop. In other words, there is a single fluid phase in the system. Therefore, to estimate the activity coefficients the experimental pressure was used as input, and the actual reactor volume was used to calculate the catalyst mass concentration at this reaction condition. It can be seen from Figure 13 that the predicted and experimental conversions profiles are in good agreement, which confirms the robustness of the reported modeling approach. Besides, it is worth pointing out that the use of a higher amount of CO_2 as solvent, has shifted the reaction equilibrium, leading to a levulinic acid conversion of 95.6% at 6:1 molar ratio.

An additional output of the kinetic calculations is the system's pressure. Which can be compared to the experimental pressure measured as the reactions proceeded. Since the general behavior is the same, and there is a total of 11 kinetic sets, all experimental and calculated temperature and pressure ramps are presented in the Appendix. There, it can be seen that, in almost all cases, pressure is overestimated by the v-T flash calculations. One reason for this is the lack of binary

interaction parameters for some of the component pairs in the reaction system. But probably, this is mostly related to the poor volumetric description offered by a classic cubic equation of state because there are density calculations implicitly in the *v*-*T* flash algorithm, to satisfy volume distribution in the reactant system (equation (12)).

It is likely that an equation of state from the Statistical Associating Fluid Theory (CHAPMAN *et al.*, 1990) (SAFT) family, which has a solid theoretical background and explicitly accounts for the hydrogen bonding phenomena, so striking in this system, would perform better not only for the pressure predictions but also in the estimation of the activities coefficients – might even matching the equilibrium conversions at different molar ratios without the additional parameter –, and we recommend it for further studies. However, the traditional cubic equations of state still have a great appeal for process simulation and optimization, particularly because they provide way faster processing and have great correlation capacity.

Overall, the experimental data collected for the $scCO_2$ assisted levulinic acid esterification with ethanol and catalyzed by Amberlyst-15 has shown the great potential of this route to produce ethyl levulinate. The presented reaction scheme leads to expressive levulinic acid conversions in fairly low residence times at most of the evaluated conditions. It was found that the levulinic acid equilibrium conversion is highly dependent on the ethanol to levulinic acid molar ratio, almost insensible to the setpoint temperature, and can be affected by the amount of $scCO_2$ added to the system. The conversion profiles, on the other hand, are highly sensitive to the temperature setpoint and catalyst loadings.

In general, the modeling approach to compute the phase partition in supercritical fluids assisted reactions proposed here performed well for this system. The Peng-Robinson equation of state with a classic quadratic mixing rule and the Boston-Mathias alpha function, which was adopted to thermodynamically represent the reaction system failed to match the equilibrium levulinic acid conversions at different ethanol to levulinic acid molar ratios. The empirical strategy with the inclusion of one additional parameter in our kinetic model fixed this issue. An activity-based Langmuir-Hinshelwood mechanism, taking the surface reaction as the rate-limiting step, was considered. It was found that ethanol and water are strongly adsorbed in the Amberlyst-15 sites, while levulinic acid and ethyl levulinate are weakly adsorbed. The proposed modeling approach led to a good representation for

all 11 kinetic sets reported in this work, over a wide range of process conditions, with an overall $RMSD$ of 4.77%.

5 FINAL REMARKS

Literature VLE data for binary pairs of the components in the studied reaction system (levulinic acid, ethanol, ethyl levulinate, water and CO_2) was retrieved from the literature and correlated using the Peng Robinson equation of state with a classic quadratic mixing rule and the Boston-Mathias alpha function. For the only non-associative pair considered (CO_2 + ethyl levulinate) a good predictive capacity was observed with this thermodynamic model. Fitting binary interaction parameters led to good correlation all binary pairs considered in this work.

The reaction kinetics of the levulinic acid ethanolic esterification assisted by $scCO_2$ and catalyzed by Amberlyst-15 was investigated. The experimental data showed promising results for the production of ethyl levulinate. A robust modeling approach to compute the phase partition in the $scCO_2$ assisted reactions was proposed and represented satisfactorily all kinetic data reported in this work. We expect the experimental data and kinetic parameters presented here to serve as starting point for further studies on the optimization and process design for the ethyl levulinate large-scale production, and, also, that the modeling strategy presented contributes to the understanding and advance of the field of $scCO_2$ assisted catalysis.

REFERENCES

BARR-DAVID, Frank; DODGE, Barnett F. Vapor-Liquid Equilibrium at High Pressures: The Systems Ethanol-Water and 2-Propanol-Water. **Journal of Chemical and Engineering Data**, [*s. l.*], v. 4, n. 2, p. 107–121, 1959. Disponível em: https://doi.org/10.1021/je60002a003

BHAT, Navya Subray; MAL, Sib Sankar; DUTTA, Saikat. Recent advances in the preparation of levulinic esters from biomass-derived furanic and levulinic chemical platforms using heteropoly acid (HPA) catalysts. **Molecular Catalysis**, [*s. l.*], v. 505, p. 111484, 2021. Disponível em: https://doi.org/10.1016/j.mcat.2021.111484

BOZELL, Joseph J.; PETERSEN, Gene R. Technology development for the production of biobased products from biorefinery carbohydrates - The US Department of Energy's "top 10" revisited. **Green Chemistry**, [*s. l.*], v. 12, n. 4, p. 539–554, 2010. Disponível em: https://doi.org/10.1039/b922014c

CHAI, Ming *et al.* Esterification pretreatment of free fatty acid in biodiesel production, from laboratory to industry. **Fuel Processing Technology**, [*s. l.*], v. 125, p. 106–113, 2014. Disponível em: https://doi.org/10.1016/j.fuproc.2014.03.025

CHAKRABARTI, Animesh; SHARMA, M M. Cationic ion exchange resins as catalyst. **Reactive Polymers**, [*s. l.*], v. 20, p. 1–45, 1993.

CHANG, Chun; XU, Guizhuan; JIANG, Xiaoxian. Production of ethyl levulinate by direct conversion of wheat straw in ethanol media. **Bioresource Technology**, [*s. l.*], v. 121, p. 93–99, 2012. Disponível em: https://doi.org/10.1016/j.biortech.2012.06.105

CHAPMAN, Walter G *et al.* New Reference Equation of State for Associating Liquids. **Industrial and Engineering Chemistry Research**, [*s. l.*], v. 29, p. 1709–1721, 1990.

CISMONDI, Martin; NDIAYE, Papa Matar; TAVARES, Frederico W. A new simple and efficient flash algorithm for T-v specifications. **Fluid Phase Equilibria**, [*s. l.*], v. 464, p. 32–39, 2018. Disponível em: https://doi.org/10.1016/j.fluid.2018.02.019

COLE-HAMILTON, David J. Homogeneous Catalysis — New Approaches to Catalyst Separation , Recovery , and Recycling. **Science**, [*s. l.*], v. 299, p. 1702, 2003. Disponível em: https://doi.org/10.1126/science.1081881

CRISTINO, A. F. *et al.* High-temperature vapour-liquid equilibrium for the water-alcohol systems and modeling with SAFT-VR: 1. Water-ethanol. **Fluid Phase Equilibria**, [*s. l.*], v. 341, p. 48–53, 2013. Disponível em: https://doi.org/10.1016/j.fluid.2012.12.014

DA SILVA JUNIOR, Vivaldo Alexandre *et al.* Effect of supercritical carbon dioxide over the esterification of levulinic acid with ethanol using montmorillonite K10 as catalyst. **Journal of CO_2 Utilization**, [*s. l.*], v. 39, p. 101158, 2020a. Disponível

em: https://doi.org/10.1016/j.jcou.2020.101158

DA SILVA JUNIOR, Vivaldo Alexandre *et al.* Effect of supercritical carbon dioxide over the esterification of levulinic acid with ethanol using montmorillonite K10 as catalyst. **Journal of CO_2 Utilization**, [*s. l.*], v. 39, n. March, p. 101158, 2020b. Disponível em: https://doi.org/10.1016/j.jcou.2020.101158

DE LA CRUZ, Mendoza J. L.; GALICIA-LUNA, Luis A. High-pressure vapor-liquid equilibria for the carbon dioxide + ethanol and carbon dioxide + propan-1-ol systems at temperatures from 322.36 K to 391.96 K. **ELDATA: The International Electronic Journal of Physico-Chemical Data**, [*s. l.*], v. 5, p. 157–164, 1999. Disponível em: http://scholar.google.com/scholar?hl=en&btnG=Search&q=intitle:High-pressure+vapor-liquid+equilibria+for+the+carbon+dioxide+++ethanol+and+carbon+dioxide+++propan-1-ol+systems+at+temperatures+from+322.36+K+to+391.96+K#0

DÉMOLIS, Alexandre; ESSAYEM, Nadine; RATABOUL, Franck. Synthesis and Applications of Alkyl Levulinates. **ACS Sustainable Chemistry & Engineering**, [*s. l.*], v. 2, n. 6, p. 1338–1352, 2014. Disponível em: https://doi.org/10.1021/sc500082n

DENG, Dongshun *et al.* Solubilities of carbon dioxide in five biobased solvents. **Journal of Chemical and Engineering Data**, [*s. l.*], v. 60, n. 1, p. 104–111, 2015. Disponível em: https://doi.org/10.1021/je500812s

DIAMANTONIS, Nikolaos I; ECONOMOU, Ioannis G. Modeling the phase equilibria of a H2O – CO_2 mixture with PC-SAFT and tPC-PSAFT equations of state. **Molecular Physics**, [*s. l.*], v. 110, n. 11–12, p. 1205–1212, 2012. Disponível em: https://doi.org/10.1080/00268976.2012.656721

EMMET REID, E. Esterification: A review of the recent past and a look towards the future. **Industrial and Engineering Chemistry**, [*s. l.*], v. 29, n. 12, p. 1344–1350, 1937. Disponível em: https://doi.org/10.1021/ie50336a007

GADAMSETTI, Sailaja *et al.* Vapor phase esterification of levulinic acid catalyzed by γ-Al2O3 supported molybdenum phosphate catalysts. **Molecular Catalysis**, [*s. l.*], v. 451, p. 192–199, 2018. Disponível em: https://doi.org/10.1016/j.mcat.2018.01.011

GALICIA-LUNA, L. A.; ORTEGA-RODRIGUEZ, A.; RICHON, D. New Apparatus for the Fast Determination of High-Pressure Vapor−Liquid Equilibria of Mixtures and of Accurate Critical Pressures. **Journal of Chemical & Engineering Data**, [*s. l.*], v. 45, n. 6, p. 1222–1222, 2000. Disponível em: https://doi.org/10.1021/je000498k

GALLETTI, Anna Maria Raspolli *et al.* Levulinic Acid Production From Waste Biomass. **BioResources**, [*s. l.*], v. 7, n. 2, p. 1824–1835, 2012. Disponível em: https://doi.org/10.1007/s40664-017-0218-9

GARVES, Klaus. Acid catalyzed degradation of cellulose in alcohols. **Journal of Wood Chemistry and Technology**, [*s. l.*], v. 8, n. 1, p. 121–134, 1988. Disponível

em: https://doi.org/10.1080/02773818808070674

GHOSH, Manik Kumer *et al.* The combustion kinetics of the lignocellulosic biofuel, ethyl levulinate. **Combustion and Flame**, [*s. l.*], v. 193, p. 157–169, 2018. Disponível em: https://doi.org/10.1016/j.combustflame.2018.02.028

GIACOMIN JUNIOR, Wanderson R. *et al.* Phase Equilibrium Measurements and Thermodynamic Modeling of the Systems (CO_2 + Ethyl Levulinate) and (CO_2 + Levulinic Acid). **Journal of Chemical and Engineering Data**, [*s. l.*], v. 64, n. 5, p. 2011–2017, 2019. Disponível em: https://doi.org/10.1021/acs.jced.8b01023

GUO, Tianmeng; QIU, Mo; QI, Xinhua. Selective conversion of biomass-derived levulinic acid to ethyl levulinate catalyzed by metal organic framework (MOF)-supported polyoxometalates. **Applied Catalysis A, General**, [*s. l.*], v. 572, p. 168–175, 2019. Disponível em: https://doi.org/10.1016/j.apcata.2019.01.004

HAMERSKI, Fabiane *et al.* Esterification reaction kinetics of acetic acid and n-pentanol catalyzed by sulfated zirconia. **International Journal of Chemical Kinetics**, [*s. l.*], v. 52, n. 8, p. 499–512, 2020. Disponível em: https://doi.org/10.1002/kin.21365

HOU, Shu Xin; MAITLAND, Geoffrey C.; TRUSLER, J. P.Martin. Measurement and modeling of the phase behavior of the (carbon dioxide + water) mixture at temperatures from 298.15 K to 448.15 K. **Journal of Supercritical Fluids**, [*s. l.*], v. 73, p. 87–96, 2013. Disponível em: https://doi.org/10.1016/j.supflu.2012.11.011

IMYEN, Thidarat *et al.* Microporous and Mesoporous Materials Investigation of ZSM-12 nanocrystals evolution derived from aluminosilicate nanobeads for sustainable production of ethyl levulinate from levulinic acid esterification with ethanol. **Microporous and Mesoporous Materials**, [*s. l.*], v. 312, p. 110768, 2021. Disponível em: https://doi.org/10.1016/j.micromeso.2020.110768

JIA, Boyu; LIU, Chunguang; QI, Xinhua. Selective production of ethyl levulinate from levulinic acid by lipase-immobilized mesoporous silica nanoflowers composite. **Fuel Processing Technology**, [*s. l.*], v. 210, p. 106578, 2020. Disponível em: https://doi.org/10.1016/j.fuproc.2020.106578

JOSHI, Hem *et al.* Ethyl levulinate: A potential bio-based diluent for biodiesel which improves cold flow properties. **Biomass and Bioenergy**, [*s. l.*], v. 35, n. 7, p. 3262–3266, 2011. Disponível em: https://doi.org/10.1016/j.biombioe.2011.04.020

KOLBE, B.; GMEHLING, J. Thermodynamic properties of ethanol + water. I. Vapour-liquid equilibria measurements from 90 to 150°C by the static method. **Fluid Phase Equilibria**, [*s. l.*], v. 23, n. 2–3, p. 213–226, 1985. Disponível em: https://doi.org/10.1016/0378-3812(85)90007-X

KONG, Xiangjin *et al.* Continuous synthesis of ethyl levulinate over Cerium exchanged phosphotungstic acid anchored on commercially silica gel pellets catalyst. **Molecular Catalysis**, [*s. l.*], v. 439, p. 180–185, 2017. Disponível em: https://doi.org/10.1016/j.mcat.2017.07.005

KONYNENBURG, P. H. V.; SCOTT, R. L. Critical Lines and Phase Equilibria

in Binary Van Der Waals Mixtures. **Philosophical Transactions of the Royal Society A: Mathematical, Physical and Engineering Sciences**, [*s. l.*], v. 298, n. 1442, p. 495–540, 1980. Disponível em: https://doi.org/10.1098/rsta.1980.0266

LE VAN MAO, R. *et al.* New process for the acid-catalyzed conversion of cellulosic biomass (AC3B) into alkyl levulinates and other esters using a unique one-pot system of reaction and product extraction. **Catalysis Letters**, [*s. l.*], v. 141, n. 2, p. 271–276, 2011. Disponível em: https://doi.org/10.1007/s10562-010-0493-y

LEAL SILVA, Jean Felipe *et al.* Making Levulinic Acid and Ethyl Levulinate Economically Viable: A Worldwide Technoeconomic and Environmental Assessment of Possible Routes. **Energy Technology**, [*s. l.*], v. 6, n. 4, p. 613–639, 2018. Disponível em: https://doi.org/10.1002/ente.201700594

LEITNER, Walter. Supercritical Carbon Dioxide as a Green Reaction Medium for Catalysis. **Acc. Chem. Res.**, [*s. l.*], v. 35, p. 746–756, 2002.

LOPEZ-ECHEVERRY, Juan Sebastian; REIF-ACHERMAN, Simon; ARAUJO-LOPEZ, Eduard. Fluid Phase Equilibria Peng-Robinson equation of state : 40 years through cubics. **Fluid Phase Equilibria**, [*s. l.*], v. 447, p. 39–71, 2017. Disponível em: https://doi.org/10.1016/j.fluid.2017.05.007

LUAN, Qing-jie *et al.* Clean and efficient conversion of renewable levulinic acid to levulinate esters catalyzed by an organic-salt of H4SiW12O40. **Process Safety and Environmental Protection**, [*s. l.*], v. 117, p. 341–349, 2018. Disponível em: https://doi.org/10.1016/j.psep.2018.05.015

MASCAL, Mark; DUTTA, Saikat. Chemical-Catalytic Approaches to the Production of Furfurals and Levulinates from Biomass. *In*: SELECTIVE CATALYSIS FOR RENEWABLE FEEDSTOCKS AND CHEMICALS. 1. ed. [*S. l.*]: Springer, 2014. p. 41–83. Disponível em: https://doi.org/10.1007/128_2014_536

MATHIAS, Paul M. A Versatile Phase Equilibrium Equation of State. **Industrial and Engineering Chemistry Process Design and Development**, [*s. l.*], v. 22, n. 3, p. 385–391, 1983. Disponível em: https://doi.org/10.1021/i200022a008

MAYADEVI, S. Reactions in supercritical carbon dioxide. **Indian Journal of Chemistry**, [*s. l.*], v. 51, p. 1298–1305, 2012.

MESHKSAR, Maryam; AFSHARIANI, Fatemeh; RAHIMPOUR, Mohammad Reza. Industrial Applications of Green Solvents for Sustainable Development of Technologies in Organic Synthesis. *In*: INAMUDDIN; ASIRI, Abdullah M (org.). **Applications of Nanotechnology for Green Synthesis**. Cham: Springer International Publishing, 2020. p. 435–455. Disponível em: https://doi.org/10.1007/978-3-030-44176-0_16

MICHELSEN, Michael L. Saturation Point Calculations. **Fluid Phase Equilibria**, [*s. l.*], v. 23, p. 181–192, 1985.

MICHELSEN, Michael L. The isothermal flash problem. part ii. phase-split calculation. **Fluid**, [*s. l.*], v. 9, p. 21–40, 1982.

MONTEIRO, M F; PEREIRA, C G. The Journal of Supercritical Fluids Description of phase equilibrium and volumetric properties for CO 2 + water and CO 2 + ethanol using the CPA equation of state. **The Journal of Supercritical Fluids**, [*s. l.*], v. 161, p. 104841, 2020. Disponível em: https://doi.org/10.1016/j.supflu.2020.104841

MORONE, Amruta; APTE, Mayura; PANDEY, R. A. Levulinic acid production from renewable waste resources: Bottlenecks, potential remedies, advancements and applications. **Renewable and Sustainable Energy Reviews**, [*s. l.*], v. 51, p. 548–565, 2015. Disponível em: https://doi.org/10.1016Zj/rser.2015.06.032

NOVITA, Felicia Januarlia; LEE, Hao-yeh; LEE, Moonyong. Energy Efficient Design of Ethyl Levulinate Reactive Distillation Process via Thermally Coupled with External Heat-Integrated Arrangement. [*s. l.*], 2017.

OGINO, Isao; SUZUKI, Yukei; MUKAI, Shin R. Esterification of levulinic acid with ethanol catalyzed by sulfonated carbon catalysts: Promotional effects of additional functional groups. **Catalysis Today**, [*s. l.*], v. 314, p. 62–69, 2018. Disponível em: https://doi.org/10.1016/j.cattod.2017.10.001

OLSON, E.S., KJELDEN, R.K., SCHLAG, A.J.; SHARMA, R.K. Levulinate Esters from Biomass Wastes. **Chemicals and Materials from Renewable Resources**, [*s. l.*], v. 784, p. 51–63, 2001. Disponível em: https://doi.org/doi:10.1021/bk-2001-0784.ch005

OTERA, Jonzo; NISHIKIDO, Joji. **Esterification: Methods, Reactions and Applications**. 2. ed. Federal Republic of Germany: Wiley-VCH, 2010.

PAL, Rammohan; SARKAR, Taradas; KHASNOBIS, Shampa. Amberlyst-15 in organic synthesis. **Arkivoc**, [*s. l.*], p. 570–609, 2012.

PENG, Ding Yu; ROBINSON, Donald B. A New Two-Constant Equation of State. **Industrial and Engineering Chemistry Fundamentals**, [*s. l.*], v. 15, n. 1, p. 59–64, 1976. Disponível em: https://doi.org/10.1021/i160057a011

PITOCHELLI, A. R. **Ion exchange catalysis and matrix effects**. Philadelphia: Rohm and Haas, 1980.

POPOVA, Margarita *et al.* Efficient solid acid catalysts based on sulfated tin oxides for liquid phase esterification of levulinic acid with ethanol. **Applied Catalysis A , General**, [*s. l.*], v. 560, p. 119–131, 2018. Disponível em: https://doi.org/10.1016/j.apcata.2018.04.041

RAMLI, Nur Aainaa Syahirah; ZAHARUDIN, Nur Hidayah; AMIN, Nor Aishah Saidina. Esterification of renewable levulic acid to levulinate esters using amberlyst-15 as a solid acid catalyst. [*s. l.*], v. 79, n. 1, p. 137–142, 2017.

RAVEENDRAN, Poovathinthodiyil; IKUSHIMA, Yutaka; WALLEN, Scott L. Polar attributes of supercritical carbon dioxide. **Accounts of Chemical Research**, [*s. l.*], v. 38, n. 6, p. 478–485, 2005. Disponível em: https://doi.org/10.1021/ar040082m

RESK, Alexander J. *et al.* Phase equilibria in systems with levulinic acid and

ethyl levulinate. **Journal of Chemical and Engineering Data**, [*s. l.*], v. 59, n. 4, p. 1062–1068, 2014. Disponível em: https://doi.org/10.1021/je400814n

RUSSO, Vincenzo *et al.* Intraparticle diffusion model to determine the intrinsic kinetics of ethyl levulinate synthesis promoted by Amberlyst-15. **Chemical Engineering Science**, [*s. l.*], v. 228, p. 115974, 2020a. Disponível em: https://doi.org/10.1016/j.ces.2020.115974

RUSSO, Vincenzo *et al.* Kinetic study of Amberlite IR120 catalyzed acid esterification of levulinic acid with ethanol: From batch to continuous operation. **Chemical Engineering Journal**, [*s. l.*], v. 401, p. 126126, 2020b. Disponível em: https://doi.org/10.1016/j.cej.2020.126126

RUSSO, Vincenzo *et al.* Kinetics and Modelling of Levulinic Acid Esterification in Batch and Continuous Reactors. **Topics in Catalysis**, [*s. l.*], v. 61, n. 18–19, p. 1856–1865, 2018. Disponível em: https://doi.org/10.1007/s11244-018-0998-y

SALVI, Harshada M; YADAV, Ganapati D. Surface functionalization of SBA-15 for immobilization of lipase and its application in synthesis of alkyl levulinates: Optimization and kinetics. **Biocatalysis and Agricultural Biotechnology**, [*s. l.*], v. 18, p. 101038, 2019. Disponível em: https://doi.org/10.1016/j.bcab.2019.101038

SAMPLE DATABASE - DIPPR801. [*S. l.*], [*s. d.*]. Disponível em: https://dippr.aiche.org/SampleDb. Acesso em: 25 mar. 2021.

SCHWAAB, Marcio; PINTO, José Carlos. Optimum reference temperature for reparameterization of the Arrhenius equation. Part 1: Problems involving one kinetic constant. **Chemical Engineering Science**, [*s. l.*], v. 62, n. 10, p. 2750–2764, 2007. Disponível em: https://doi.org/10.1016/j.ces.2007.02.020

SCURTO, Aaron M.; HUTCHENSON, Keith; SUBRAMANIAM, Bala. Gas-Expanded Liquids: Fundamentals and Applications. *In*: GAS-EXPANDED LIQUIDS AND NEAR-CRITICAL MEDIA. Washington, DC: ACS Books Department, 2009. p. 378.

SECUIANU, Catinca; FEROIU, Viorel; GEANĂ, Dan. Phase behavior for carbon dioxide + ethanol system: Experimental measurements and modeling with a cubic equation of state. **Journal of Supercritical Fluids**, [*s. l.*], v. 47, n. 2, p. 109–116, 2008. Disponível em: https://doi.org/10.1016/j.supflu.2008.08.004

SERT, Murat. Catalytic effect of acidic deep eutectic solvents for the conversion of levulinic acid to ethyl levulinate. **Renewable Energy**, [*s. l.*], v. 153, p. 1155–1162, 2020. Disponível em: https://doi.org/10.1016/j.renene.2020.02.070

SHRIKHANDE, Savyasachi *et al.* Intensification and analysis of ethyl levulinate production process having a reactive distillation through vapor recompression and bottom flash techniques. **Chemical Engineering & Processing: Process Intensification**, [*s. l.*], v. 156, p. 108081, 2020. Disponível em: https://doi.org/10.1016/j.cep.2020.108081

SHYU, Guor-shiarn *et al.* Carbon dioxide-water phase equilibria results from the Wong-Sandler combining rules. **Fluid Phase Equilibria**, [*s. l.*], v. 130, p. 73–85,

1997.

SIEVERS, Carsten *et al.* Phenomena affecting catalytic reactions at solid−Liquid interfaces. **ACS Catalysis**, [*s. l.*], v. 6, n. 12, 2016. Disponível em: https://doi.org/10.1021/acscatal.6b02532

SIRSAM, Rajkumar; HANSORA, Dharmesh; USMANI, Ghayas A. A Mini-Review on Solid Acid Catalysts for Esterification Reactions. **Journal of The Institution of Engineers (India): Series E**, [*s. l.*], v. 97, n. 2, p. 167–181, 2016. Disponível em: https://doi.org/10.1007/s40034-016-0078-4

SKOUTA, Rachid. Selective chemical reactions in supercritical carbon dioxide, water, and ionic liquids. **Green Chemistry Letters and Reviews**, [*s. l.*], v. 2, n. 3, p. 121–156, 2009. Disponível em: https://doi.org/10.1080/17518250903230001

SOH, Lindsay *et al.* Role of CO_2 in Mass Transfer, Reaction Kinetics, and Interphase Partitioning for the Transesterification of Triolein in an Expanded Methanol System with Heterogeneous Acid Catalyst. **ACS Sustainable Chemistry & Engineering**, [*s. l.*], v. 3, p. 2669–2677, 2015. Disponível em: https://doi.org/10.1021/acssuschemeng.5b00472

SUBRAMANLAMR, Bala; MCHUGH, Mark A. Reactions in Supercritical Fluids-a Review. **Industrial and Engineering Chemistry Process Design and Development**, [*s. l.*], v. 25, n. 1, p. 1–12, 1986. Disponível em: https://doi.org/10.1021/i200032a001

SUZUKI, Kazuhiko *et al.* Isothermal Vapor-Liquid Equilibrium Data for Binary Systems at High Pressures: Carbon Dioxide-Methanol, Carbon Dioxide-Ethanol, Carbon Dioxide-1-Propanol, Methane-Ethanol, Methane-1-Propanol, Ethane-Ethanol, and Ethane-1-Propanol Systems. **Journal of Chemical and Engineering Data**, [*s. l.*], v. 35, n. 1, p. 63–66, 1990. Disponível em: https://doi.org/10.1021/je00059a020

TROMBETTONI, Valeria *et al.* Efficient Catalytic Upgrading of Levulinic Acid into Alkyl Levulinates by Resin-Supported Acids and Flow Reactors. **Catalysts**, [*s. l.*], v. 7, p. 235, 2017. Disponível em: https://doi.org/10.3390/catal7080235

TSAI, Chia-Ying. **Kinetic behavior study on the synthesis of ethyl levulinate over heterogeneous catalyst**. 161 f. 2014. - National Taiwan University of Science and Technology, [*s. l.*], 2014.

V. GROTE, A. Freiherr; TOLLENS, B. Ueber die bei Einwirkung von Schwefelsäure auf Zucker entstehende Levulinsäure. **Berichte der deutschen chemischen Gesellschaft**, [*s. l.*], v. 7, n. 2, p. 1375–1381, 1874. Disponível em: https://doi.org/10.1002/cber.187400702134

VÁZQUEZ-CASTILLO, José A *et al.* Optimally designed reactive distillation processes for eco-efficient production of ethyl levulinate. **J Chem Technol Biotechnol**, [*s. l.*], v. 94, p. 2131–2140, 2019. Disponível em: https://doi.org/10.1002/jctb.6033

WACŁAWEK, Stanisław; PADIL, Vinod V.T.; CERNIK, Miroslav. Major advances and challenges in heterogeneous catalysis for environmental applications:

A review. **Ecological Chemistry and Engineering S**, [*s. l.*], v. 25, n. 1, p. 9–34, 2018. Disponível em: https://doi.org/10.1515/eces-2018-0001

WANG, Zhi Wei *et al.* Performance investigations of a diesel engine using ethyl levulinate-diesel blends. **BioResources**, [*s. l.*], v. 7, n. 4, p. 5972–5982, 2012. Disponível em: https://doi.org/10.15376/biores.7.4.5972-5982

ZAINOL, Muzakkir Mohammad *et al.* Effects of thermal treatment on carbon cryogel preparation for catalytic esterification of levulinic acid to ethyl levulinate. **Fuel Processing Technology**, [*s. l.*], v. 167, p. 431–441, 2017. Disponível em: https://doi.org/10.1016/j.fuproc.2017.07.028

ZAINOL, Muzakkir Mohammad *et al.* Synthesis and characterization of porous microspherical ionic liquid carbon cryogel catalyst for ethyl levulinate production. **Diamond & Related Materials**, [*s. l.*], v. 95, p. 154–165, 2019. Disponível em: https://doi.org/10.1016/j.diamond.2019.04.014

ZHAO, Shiqiang *et al.* Direct conversion of carbohydrates into ethyl levulinate with potassium phosphotungstate as an efficient catalyst. **Catalysts**, [*s. l.*], v. 5, n. 4, p. 1897–1910, 2015. Disponível em: https://doi.org/10.3390/catal5041897

ZHU, Weina *et al.* Kinetics of glucose ethanolysis catalyzed by extremely low sulfuric acid in ethanol medium. **Chinese Journal of Chemical Engineering**, [*s. l.*], v. 22, n. 2, p. 238–242, 2014. Disponível em: https://doi.org/10.1016/S1004-9541(14)60049-5

ZIYANG, Zhang; HIDAJAT, K.; RAY, Ajay K. Determination of adsorption and kinetic parameters for methyl tert-butyl ether synthesis from tert-butyl alcohol and methanol. **Journal of Catalysis**, [*s. l.*], v. 200, n. 2, p. 209–221, 2001. Disponível em: https://doi.org/10.1006/jcat.2001.3180

APPENDIX I – TEMPERATURE AND PRESSURE PROFILES

Here the experimental and simulated temperature and pressure profiles are presented, as discussed in section 4.2.

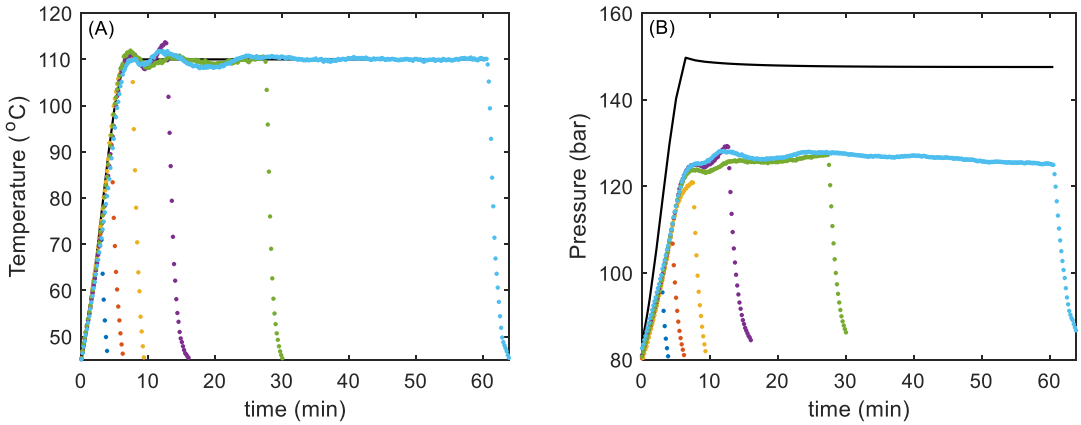

Figure S1: Experimental (colored dots) and simulated (continuous black lines) temperature (A) and pressure (B) profiles, for the K1 kinetic set, according to Table 4. The experimental conditions were: ethanol to levulinic acid molar ratio of 1:1; catalyst to acid mass relation of 5 wt%; temperature setpoint of 110 °C; and CO_2 to reactants mass ratio of 3:1.

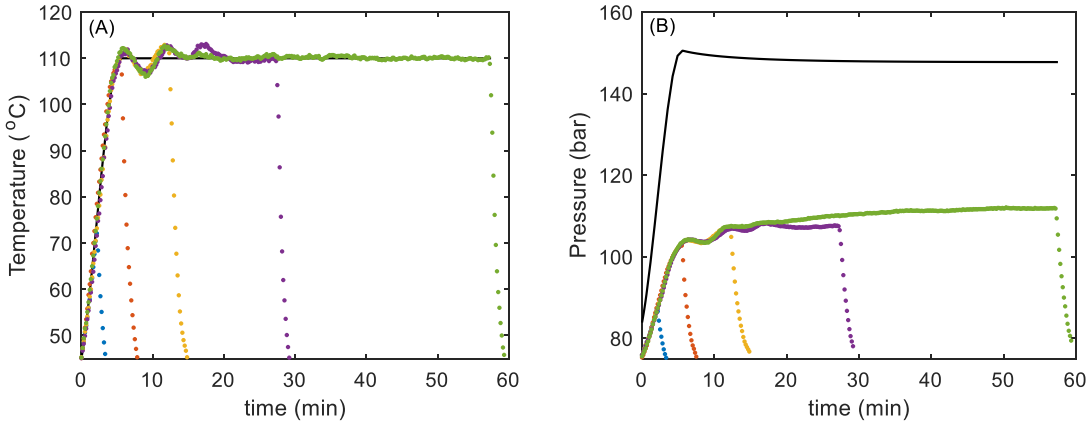

Figure S2: Experimental (colored dots) and simulated (continuous black lines) temperature (A) and pressure (B) profiles, for the K2 kinetic set, according to Table 4. The experimental conditions were: ethanol to levulinic acid molar ratio of 3:1; catalyst to acid mass relation of 5 wt%; temperature setpoint of 110 °C; and CO_2 to reactants mass ratio of 3:1.

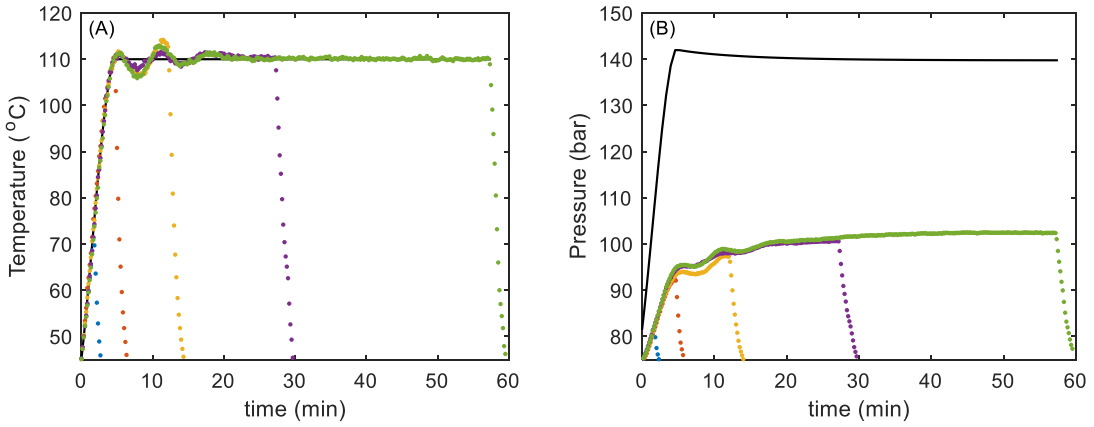

Figure S3: Experimental (colored dots) and simulated (continuous black lines) temperature (A) and pressure (B) profiles, for the K3 kinetic set, according to Table 4. The experimental conditions were: ethanol to levulinic acid molar ratio of 6:1; catalyst to acid mass relation of 5 wt%; temperature setpoint of 110 °C; and CO_2 to reactants mass ratio of 3:1.

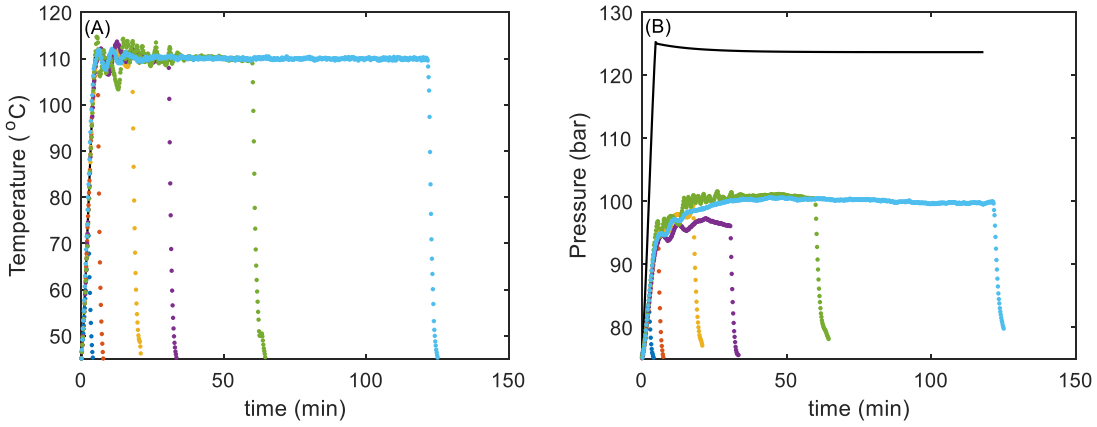

Figure S4: Experimental (colored dots) and simulated (continuous black lines) temperature (A) and pressure (B) profiles, for the K4 kinetic set, according to Table 4. The experimental conditions were: ethanol to levulinic acid molar ratio of 9:1; catalyst to acid mass relation of 5 wt%; temperature setpoint of 110 °C; and CO_2 to reactants mass ratio of 3:1.

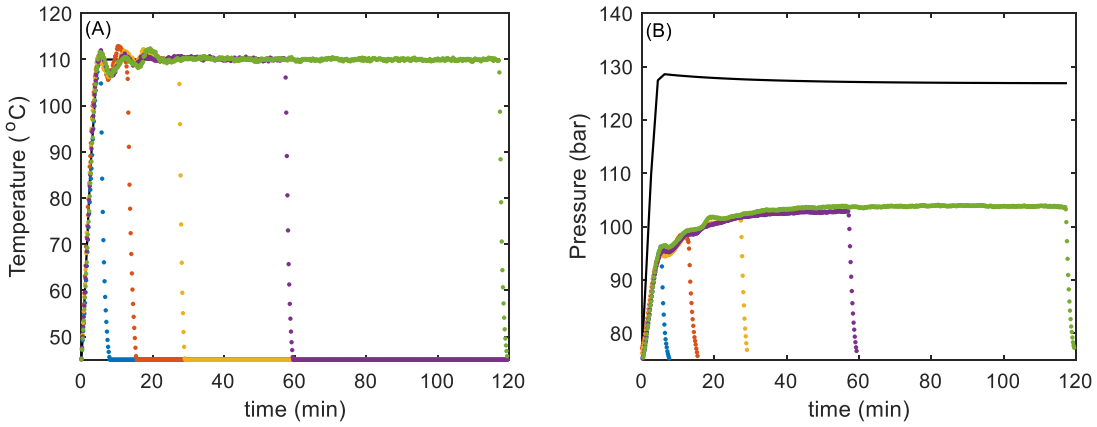

Figure S5: Experimental (colored dots) and simulated (continuous black lines) temperature (A) and pressure (B) profiles, for the K5 kinetic set, according to Table 4. The experimental conditions were: ethanol to levulinic acid molar ratio of 6:1; catalyst to acid mass relation of 2 wt%; temperature setpoint of 110 °C; and CO_2 to reactants mass ratio of 3:1.

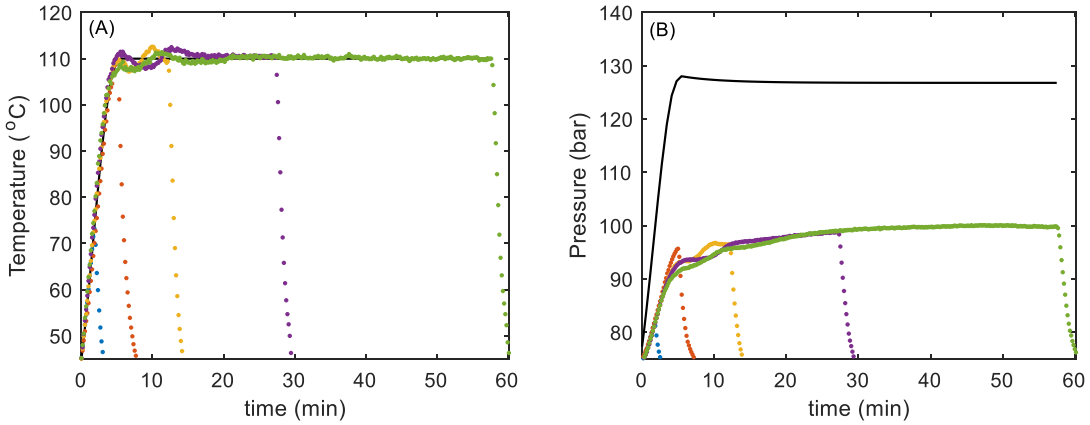

Figure S6: Experimental (colored dots) and simulated (continuous black lines) temperature (A) and pressure (B) profiles, for the K6 kinetic set, according to Table 4. The experimental conditions were: ethanol to levulinic acid molar ratio of 6:1; catalyst to acid mass relation of 10 wt%; temperature setpoint of 110 °C; and CO_2 to reactants mass ratio of 3:1.

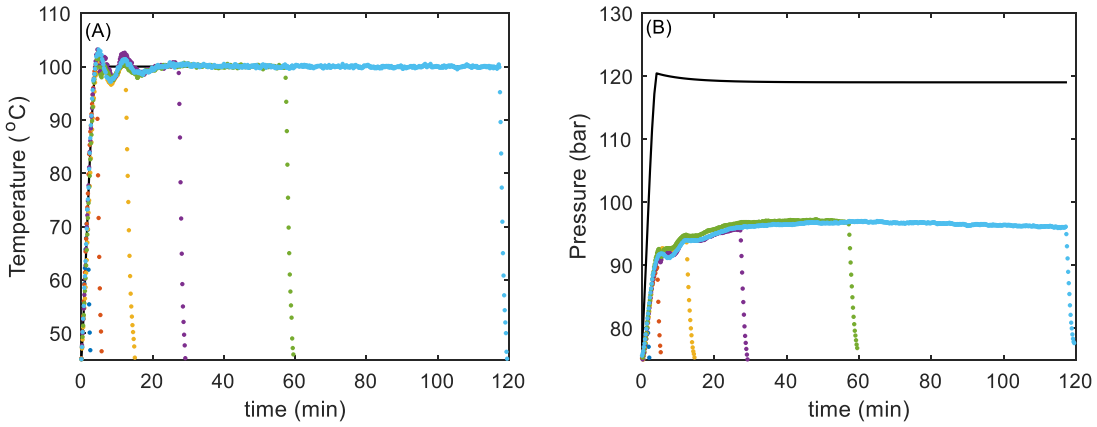

Figure S7: Experimental (colored dots) and simulated (continuous black lines) temperature (A) and pressure (B) profiles, for the K7 kinetic set, according to Table 4. The experimental conditions were: ethanol to levulinic acid molar ratio of 6:1; catalyst to acid mass relation of 10 wt%; temperature setpoint of 100 °C; and CO_2 to reactants mass ratio of 3:1.

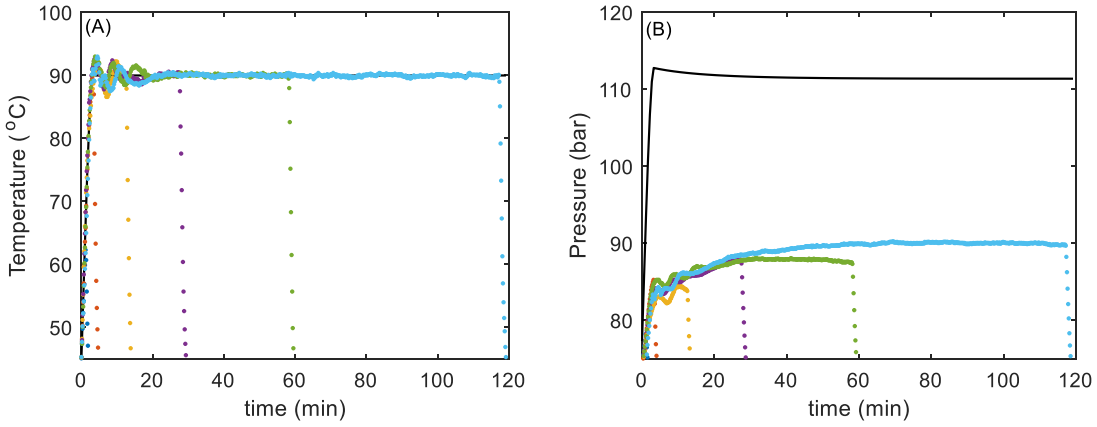

Figure S8: Experimental (colored dots) and simulated (continuous black lines) temperature (A) and pressure (B) profiles, for the K8 kinetic set, according to Table 4. The experimental conditions were: ethanol to levulinic acid molar ratio of 6:1; catalyst to acid mass relation of 10 wt%; temperature setpoint of 90 °C; and CO_2 to reactants mass ratio of 3:1.

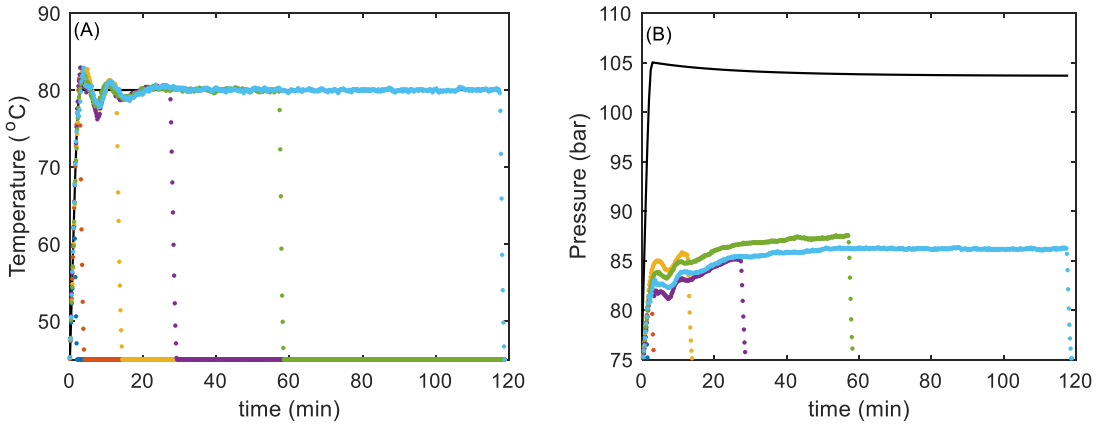

Figure S9: Experimental (colored dots) and simulated (continuous black lines) temperature (A) and pressure (B) profiles, for the K9 kinetic set, according to Table 4. The experimental conditions were: ethanol to levulinic acid molar ratio of 6:1; catalyst to acid mass relation of 10 wt%; temperature setpoint of 80 °C; and CO_2 to reactants mass ratio of 3:1.

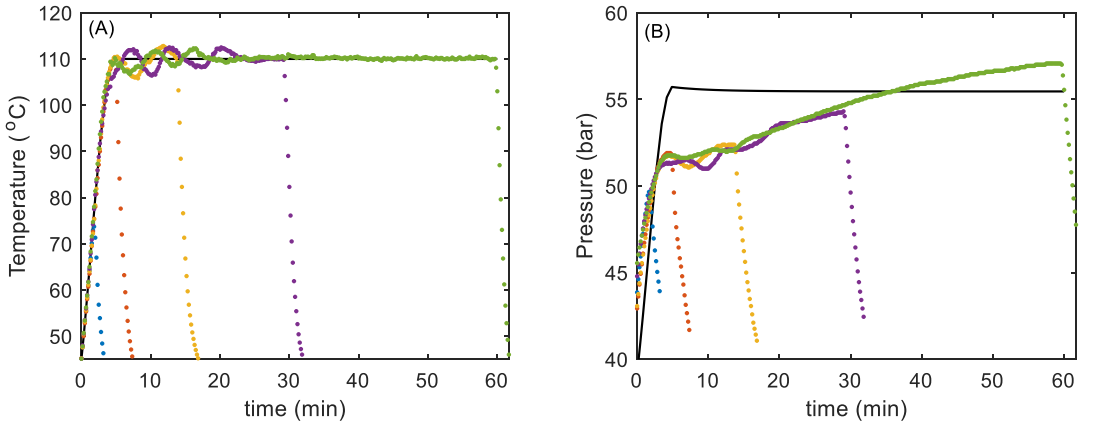

Figure S10: Experimental (colored dots) and simulated (continuous black lines) temperature (A) and pressure (B) profiles, for the K10 kinetic set, according to Table 4. The experimental conditions were: ethanol to levulinic acid molar ratio of 6:1; catalyst to acid mass relation of 10 wt%; temperature setpoint of 110 °C; and CO_2 to reactants mass ratio of 1:1.

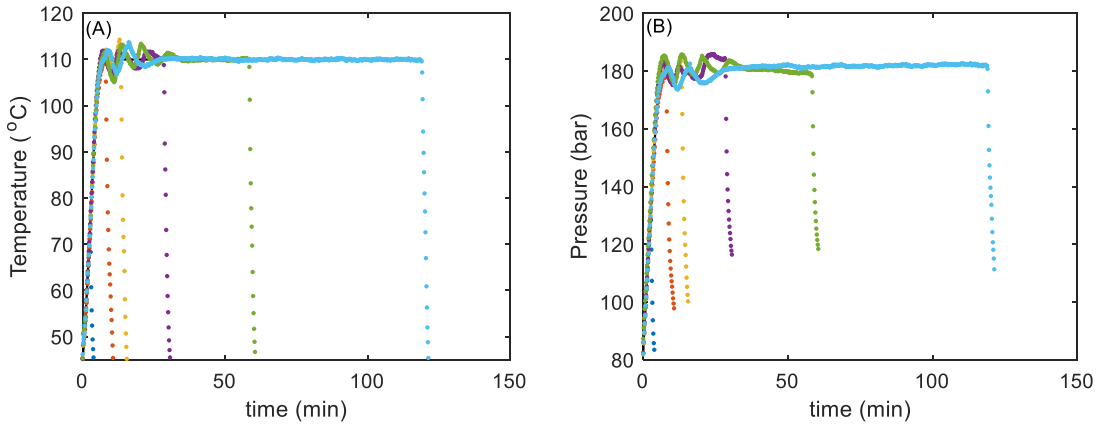

Figure S11: Experimental (colored dots) and simulated (continuous black lines) temperature (A) and pressure (B) profiles, for the K10 kinetic set, according to Table 4. The experimental conditions were: ethanol to levulinic acid molar ratio of 6:1; temperature setpoint of 110 °C; catalyst to acid mass relation of 10 wt%; and CO_2 to reactants mass ratio of 5:1.